MASTERARBEIT | MASTER'S THESIS

Titel | Title

The handbook of IMF observations with the ELT

verfasst von | submitted by

Maximilian Köcher BSc

angestrebter akademischer Grad | in partial fulfilment of the requirements for the degree of

Master of Science (MSc)

Wien | Vienna, 2025

Studienkennzahl lt. Studienblatt | Degree programme code as it appears on the student record sheet:	UA 066 861
Studienrichtung lt. Studienblatt | Degree programme as it appears on the student record sheet:	Masterstudium Astronomy
Betreut von | Supervisor:	Dr. Kieran Leschinski MSc

Abstract

Objective: The Initial Mass Function (IMF) is a fundamental parameter in astrophysics that describes the mass distribution of stars in a newly forming population. Although there are several empirical formulations of the IMF, its true form remains unknown. A significant reason for this uncertainty is that current telescopes, such as the 8-meter VLT, lack the capability to detect low-mass stars (including "brown dwarfs") in distant star clusters. This limitation, however, is expected to change with the advent of a new generation of large telescopes, like the 39-meter Extremely Large Telescope (ELT).

Open star clusters offer ideal environments for IMF studies, as they consist of stars that formed around the same time, creating a uniform population with a range of stellar masses. By determining the masses of all stars within a cluster, an estimate of the IMF can be derived.

This research project aims to create an "Initial Mass Function Handbook" specifically designed for future IMF studies with the ELT. The handbook serves as a catalog of open star clusters in the Milky Way, providing the key parameters required for future ELT observations.

Methods: For this project, a catalog of over 1,000 Milky Way open star clusters suitable for ELT observations was compiled, largely based on data from the Milky Way Star Cluster (MWSC) catalog. Simulated near-infrared observations in the J and Ks bands were then generated for each cluster using the MICADO instrument on the ELT, employing the ScopeSim toolkit. These simulations produced images in both filters for each star cluster in the dataset, which were then analyzed and visually evaluated.

Results: The results highlight the advantages of MICADO for observing high-density star clusters, particularly those near the Galactic center. While current instruments like HAWK-I are suitable for observing nearby, low-density clusters, MICADO is essential for clusters located beyond approximately 3 kpc. Even with MICADO, some challenges remain, such as the photometric complexities introduced by its segmented mirror design. Additionally, MICADO's relatively small field of view (53x53 arcsec) often requires substantial observing time to cover entire star clusters comprehensively.

The IMF Handbook provides essential support for future observational planning and instrument selection for IMF studies. As a practical resource, this handbook is intended to assist astronomers significantly once the Extremely Large Telescope is operational.

Kurzfassung

Ziel: Die Initial Mass Function (kurz: IMF) ist eine zentrale Größe in der Astrophysik, welche die Massenverteilung der Sterne in einer neu entstehenden Sternpopulation beschreibt. Es gibt mehrere empirische Beschreibungen der IMF, doch bis zum heutigen Tag ist die wahre Form der IMF unbekannt. Gründe dafür sind, dass aktuelle Teleskope wie das VLT mit 8m Spiegeldurchmesser nicht in der Lage sind, Sterne mit geringer Masse (sogenannte "brown dwarfs") in weiter entfernten Sternhaufen zu detektieren. Dies wird sich allerdings ändern, sobald uns die neue Generation von Großteleskopen wie das 39m Extremely Large Telescope (ELT) zur Verfügung steht.

Besonders geeignet für die Untersuchung der IMF ist die Beobachtung von offenen Sternhaufen. Diese haben den Vorteil, dass alle Sterne ungefähr zur gleichen Zeit entstanden sind. Es handelt sich dabei um eine einheitliche Sternpopulation mit verschiedenen Sternmassen. Durch Bestimmung aller Massen in einem Sternhaufen kann die IMF abgeschätzt werden.

Das Ziel dieser Masterarbeit ist die Fertigung eines "Initial Mass Function Handbuch" für ELT Beobachtungen. Das Handbuch soll ein Katalog von offenen Sternhaufen der Milchstraße sein mit allen charakteristischen Größen, die für zukünftige ELT Beobachtungen benötigt werden.

Methoden: Für dieses Projekt wurde ein Katalog von mehr als 1000 offenen Sternhaufen der Milchstraße erstellt, welche für ELT Beobachtungen geeignet sind. Die Daten stammen dabei zu einem großen Teil vom Milky Way Star Cluster Katalog (MWSC). Mit dem ScopeSim Toolkit wurden anschließend nahinfrarote Beobachtungen im J- und Ks-Band mit dem ELT Instrument MICADO simuliert. Dabei entstanden Aufnahmen in beiden Filtern von allen Sternhaufen des Datensatzes. Diese Aufnahmen wurden anschließend analysiert und visuell ausgewertet.

Resultate: Die Ergebnisse verdeutlichen die Vorteile von MICADO bei der Beobachtung von Sternhaufen mit hoher Sterndichte, insbesondere im galaktischen Zentrum. Während aktuelle Instrumente wie HAWK-I geeignet sind für die Beobachtung von nahen und wenig dichten Sternhaufen, benötigt es MICADO für alles was über Distanzen von etwa 3 kpc hinausgeht. Doch auch mit MICADO gibt es einige Probleme zu bewältigen, zum Beispiel bringt der segmentierte Spiegel neue Herausforderungen bei der Photometrie mit sich. Das Sichtfeld von MICADO ist mit 53x53 arcsec sehr klein, um einen Sternhaufen vollständig zu beobachten, benötigt es teilweise immens viel Beobachtungszeit.

Das IMF-Handbuch soll die zukünftige Beobachtungsplanung und Instrumentenwahl für Studien bezüglich der Initial Mass Function unterstützen. Es ist ein praktisches Werkzeug, das hoffentlich bei der Fertigstellung des Extremely Large Teleskops Astronomen von großem Nutzen sein wird.

Contents

List of Tables

List of Figures

1. Introduction

For a long time, the study of star clusters has been essential to comprehending the evolution of stars and galaxies. Models of star formation, dynamics, and stellar mass distribution can all be tested in natural laboratories - star clusters, which are dense collections of stars constrained by gravitational pull. The Initial Mass Function (IMF) is a fundamental quantity in these studies that characterizes the distribution of stellar masses during their formation. In addition to its effects on star cluster evolution, the IMF also affects the chemical enrichment of galaxies and the overall evolution of the universe. Still, at this time little is known about the true nature of the IMF, particularly with regard to the lower-mass segment (brown dwarfs).

Upcoming advancements in astronomy will allow us to observe compact and distant star clusters with incredible detail. New instruments such as the *Multi-AO Imaging Camera for Deep Observations* (MICADO) on the future Extremely Large Telescope (ELT) and the *James Webb Space Telescope* (JWST), which is already in operation, will help us study crowded star clusters in ways that current instruments cannot. These new tools will make it possible to examine star clusters in the center of our galaxy and nearby galaxies, giving us a clearer view of the Initial Mass Function (IMF) and helping us understand star clusters better [Leschinski and Alves, 2020].

This thesis is organized as follows:

- Chapter 1 provides a comprehensive review of the literature on IMF studies, discussing the foundational work and recent advancements as well as an overview on the instrumentation like MICADO of the ELT.
- Chapter 2 is a detailed description of the methodology used in this study, including the utilized data set of open star clusters in the Milky Way, the simulations conducted and the analysis techniques employed.
- Chapter 3 presents the results of the simulations and data compilation.
- Chapter 4 is a discussion of the problems, possibilities and some suggestions for future research and observations regarding IMF studies.
- Chapter 5 is the conclusion of this research project.

1.1. Research Motivation and Goals

Despite the many advances in astronomical instrumentation, the study of the IMF in crowded fields remains a challenging problem. Crowding distances, star densities, and the limiting magnitude of instruments introduce significant challenges to accurately measure the distribution of stellar masses. This research project addresses these issues by compiling a comprehensive IMF handbook, utilizing a large simulation on open clusters in the Milky Way.

The goals of the project are the following:

- Compile a detailed analysis of over 1000 star clusters using simulated data.
- Explore the impact of different instruments (MICADO, JWST, and HAWK-I) on observing crowded stellar fields.
- Provide new insights into the crowding distance limitations for each instrument and the implications for IMF studies.

1.2. Overview of the Initial Mass Function (IMF)

The Initial Mass Function (IMF) has implications in almost all fields of astrophysics. It describes the distribution of stellar masses at birth in a population of stars. It plays a fundamental role in shaping our understanding of star formation, the evolution of galaxies, and the chemical enrichment of the universe. Various formulations of the IMF have been proposed over the years, each with distinct implications for the mass distribution of stars in different environments. This section provides detailed descriptions of the three most widely-used IMF forms: the Salpeter IMF [Salpeter, 1955], the Kroupa IMF [Kroupa, 2001], and the Chabrier IMF [Chabrier, 2003], followed by an overview on IMF Variability and Environmental Dependence.

1.2.1. Salpeter IMF

The Salpeter Initial Mass Function (IMF), introduced by Edwin E. Salpeter in 1955, is one of the earliest and simplest formulations of the IMF. Salpeter proposed a power-law distribution of stellar masses, which has since become foundational in studies of star formation rates, the mass distribution of stars, and the evolution of galaxies [Salpeter, 1955]. Despite its simplicity, the Salpeter IMF remains a widely used approximation, particularly for populations of high-mass stars.

Equation

The Salpeter IMF is mathematically described by a power-law function:

$$\xi(m) = \xi_0 m^{-\alpha}$$

where:

- $\xi(m)$ is the number of stars per unit mass interval,
- ξ_0 is a normalization constant,
- m is the mass of the star, typically measured in units of solar masses ($M_\odot$),
- $\alpha = 2.35$ is the power-law exponent proposed by Salpeter.

Mass Range

The Salpeter IMF typically covers a mass range from around 0.4 to 10 solar masses ($M_\odot$), capturing a broad spectrum from low-mass M dwarfs to high-mass O-type stars. It follows a power-law, meaning low-mass stars are more common than high-mass stars. However, the Salpeter IMF is not well-defined for very low-mass objects, such as brown dwarfs. This creates uncertainty in the formation and frequency of these substellar objects, making it harder to accurately model the complete mass distribution, particularly in environments where low-mass stars and brown dwarfs may dominate.

1.2.2. Kroupa IMF

The Kroupa IMF, introduced by Pavel Kroupa in 2001, provides a more refined description of the stellar mass distribution, particularly for low-mass stars and brown dwarfs. Unlike the Salpeter IMF, which follows a single power law, the Kroupa IMF uses a broken power-law to better match observed stellar populations across a wider mass range [Kroupa, 2001]. This formulation accounts for the flattening of the IMF at lower masses, which is crucial for accurately modeling the frequency of substellar objects and low-mass stars in star-forming regions.

Equation

The Kroupa IMF is described by a piecewise power-law function:

$$\xi(m) \propto \begin{cases} m^{-0.3} & \text{for } 0.01 \leq m < 0.08 M_\odot, \\ m^{-1.3} & \text{for } 0.08 \leq m < 0.5 M_\odot, \\ m^{-2.3} & \text{for } m \geq 0.5 M_\odot. \end{cases}$$

This segmented power-law reflects the fact that the distribution of stellar masses flattens significantly at very low masses (below 0.08 $M_\odot$), representing brown dwarfs and low-mass stars. The steeper slopes for higher masses account for the decreasing frequency of more massive stars.

Mass Range

The Kroupa IMF spans a wide mass range, from substellar objects like brown dwarfs (with masses less than 0.08 $M_\odot$) to massive stars exceeding 100 $M_\odot$. This flexibility allows it to more accurately describe the full range of stellar masses observed in star-forming regions, making it particularly useful for studying the formation and evolution of diverse stellar populations, including those in the Milky Way and other galaxies.

1.2.3. Chabrier IMF

The Chabrier IMF, proposed by Gilles Chabrier in 2003 [Chabrier, 2003], offers an alternative to the Kroupa IMF, particularly at the low-mass end. Instead of using a piecewise power-law, Chabrier proposed a log-normal distribution for stellar masses below 1 $M_\odot$, which better reflects the observed distribution of low-mass stars. This model is widely used in both observational and theoretical studies of stellar populations.

Equation

The Chabrier IMF is expressed as a log-normal distribution for low-mass stars ($m < 1M_\odot$):

$$\xi(logm) \propto \frac{1}{m} \exp\left(-\frac{(\log m - \log m_c)^2}{2\sigma^2}\right)$$

where:

- $m_c \approx 0.2M_\odot$ is the characteristic mass,
- $\sigma \approx 0.55$ is the width of the log-normal distribution.

For higher-mass stars, Chabrier adopts a power-law similar to the Salpeter IMF:

$$\xi(m) \propto m^{-2.3} \quad \text{for } m > 1M_\odot.$$

1.2.4. Comparison of IMFs

Figure 1.1 shows a comparison of the Salpeter, Kroupa, and Chabrier IMFs, which focuses on the lower mass range spanning from 0.013 to 5 $M_\odot$. While the Salpeter IMF follows a single power-law across all mass ranges, both the Kroupa and Chabrier IMFs introduce modifications at the low-mass end to account for the flattening observed in star formation regions.

This low-mass regime includes the transition from stars to brown dwarfs, marked at 0.08 $M_\odot$ [Burrows et al., 2001]. Objects below this threshold are unable to sustain hydrogen fusion in their cores and are classified as brown dwarfs. At the lower end of the mass scale, brown dwarfs capable of fusing deuterium are found above approximately 0.013 $M_\odot$ (13 times the mass of Jupiter), while objects below this are considered planetary-mass objects [Spiegel et al., 2011]. Both the Kroupa and Chabrier IMFs predict a much shallower slope at these low masses, reflecting the greater abundance of low-mass stars and substellar objects.

However, despite these adjustments, the true nature of the IMF at low masses remains uncertain. Observations at these masses are challenging due to the intrinsic faintness of low-mass stars, crowding in dense stellar environments, and the limitations of current

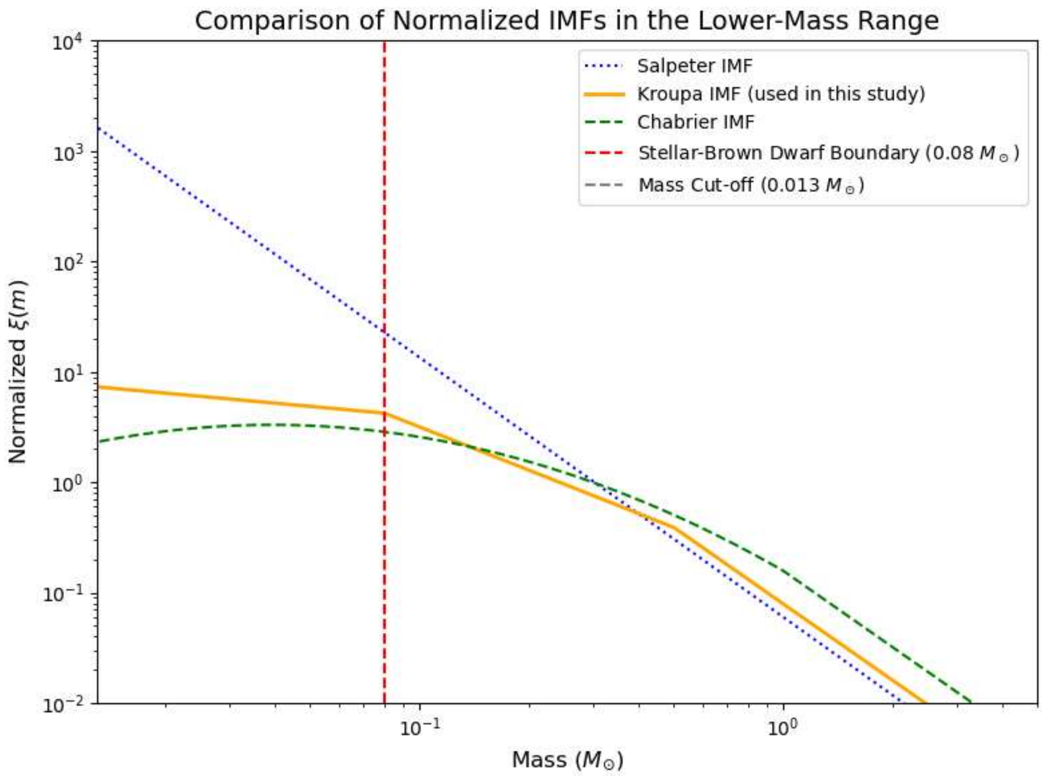

Figure 1.1.: Comparison of normalized IMFs in the lower-mass range (0.01 to 5 $M_\odot$). The Salpeter IMF (blue, dotted), Kroupa IMF (orange, solid), and Chabrier IMF (green, dashed) are shown. The Stellar-Brown Dwarf Boundary at 0.08 $M_\odot$ (red dashed line) marks the transition between stars and substellar objects. The mass cut-off at 0.013 $M_\odot$ represents the lower limit for brown dwarfs. The Kroupa IMF is highlighted because it is used in this study. This low-mass segment is particularly relevant as IMFs differ significantly and remain poorly understood in this regime, highlighting the need for further investigation.

observational instruments. This uncertainty is further compounded in distant star-forming regions and environments with extreme conditions, such as the Galactic center or low-metallicity galaxies. Future observations with instruments like the ELT and MICADO will provide the resolution and sensitivity needed to probe these regions and help clarify the IMF at the low-mass end.

1.2.5. IMF Variability and Environmental Dependence

The Initial Mass Function (IMF) has traditionally been regarded as universal, with a consistent distribution across diverse star-forming environments. However, recent studies suggest that factors such as metallicity, temperature, stellar density, and star formation rate may influence the IMF, leading to variations in different environments.

[Bastian et al., 2010] conducted a comprehensive review of observational and theoretical evidence, concluding that although some studies suggest IMF variations, most observed IMFs remain similar across environments. This supports a largely universal IMF, especially within the Milky Way and nearby galaxies. However they acknowledged that extreme conditions—such as those found in high-mass starburst regions—might produce a "top-heavy" IMF and emphasized the need for further, more precise data to clarify these potential variations.

Expanding on this, [Marks et al., 2012] found evidence that high-density, low-metallicity environments, such as globular clusters, are more likely to yield a top-heavy IMF. They argued that these conditions favor massive star formation, likely due to reduced cooling and modified fragmentation processes in dense, metal-poor regions.

Additionally, simulations of star formation support the idea that molecular cloud fragmentation and accretion processes may impact the IMF, suggesting that physical conditions could lead to systematic variations [Offner et al., 2014]. They concluded that, while the IMF is generally consistent, certain extreme environments may cause slight deviations, underscoring a near-universal IMF with rare, localized exceptions.

Variations in the IMF have significant implications for interpreting stellar populations and modeling galactic evolution. A top-heavy IMF enhances supernova rates and feedback, potentially accelerating galaxy growth and interstellar medium enrichment. Conversely, an IMF skewed toward low-mass stars results in a higher contribution to the galactic stellar mass but produces fewer luminous stars, affecting energy output and feedback processes.

Given these potential variations, studying the IMF across different environments remains a critical area of astrophysical research. This thesis explores the IMF in crowded stellar fields through simulations, aiming to provide insights into its characteristics in high-density environments that challenge traditional observational methods, such as star clusters with high stellar densities.

1.3. Introduction to Key Instruments

Advances in telescope technology are opening up new possibilities for studying dense star fields and accurately measuring the Initial Mass Function (IMF). Among the next generation of observatories, the **Extremely Large Telescope (ELT)** stands out. With its enormous 39-meter mirror, the ELT will be the largest optical and near-infrared telescope in the world, equipped to capture extremely detailed images. Its first-light instrument, **MICADO**, will use adaptive optics to achieve high-resolution imaging, ideal for examining tightly packed stars in star clusters and galactic centers.

The **James Webb Space Telescope (JWST)**, which is already in operation, also plays a crucial role in IMF studies. Observing from space, JWST provides highly sensitive infrared data that helps astronomers explore distant and dusty regions. With instruments like NIRCam, JWST can see deep into areas that are challenging for ground-based telescopes.

The **Very Large Telescope (VLT)** and its **HAWK-I** instrument remain important in advancing our understanding of stellar populations. HAWK-I's wide field of view and adaptive optics capabilities make it well-suited for studying nearby star clusters, despite its lower limiting magnitude and resolution compared to next-generation instruments like **MICADO** on the ELT or **NIRCam** on the JWST. Using all three instruments together will provide unprecedented insights into the lower end of the Initial Mass Function (IMF), revealing details about low-mass stars and substellar objects in diverse galactic environments.

1.3.1. The Extremely Large Telescope (ELT)

The **Extremely Large Telescope (ELT)**, currently under construction by the European Southern Observatory (ESO) at Cerro Armazones in Chile, is set to become the largest optical and near-infrared telescope in the world with its 39-meter primary mirror [European Southern Observatory (ESO), 2024]. Scheduled for first light in 2028, the ELT's massive collecting area and advanced optical design will make it capable of capturing extremely faint, distant objects, providing unprecedented detail in crowded stellar regions like star clusters and the Galactic center.

The ELT uses a **five-mirror design** incorporating advanced **adaptive optics (AO)** for real-time correction of atmospheric distortions. This design, along with a deformable mirror (M4), will enable diffraction-limited imaging, achieving resolutions up to 400 times sharper than Hubble in the infrared. The telescope will operate across a wavelength range of **0.37 to 14 microns**, covering visible to mid-infrared wavelengths.

The ELT will host several advanced instruments, each designed for specialized observations:

- **MICADO**: A high-resolution near-infrared imager optimized for crowded fields, crucial for IMF studies in dense environments.
- **HARMONI**: An integral field spectrograph for spatially-resolved spectroscopy, suitable for detailed analysis of galaxies and stellar populations.
- **METIS**: A mid-infrared imager and spectrograph for observing cooler, more obscured regions.
- **MORFEO**: An AO module that will work with MICADO, enhancing resolution and stability in crowded fields by compensating for atmospheric turbulence.
- **ANDES**: A high-resolution spectrograph for detailed spectral analysis, ideal for studying exoplanet atmospheres and stellar compositions.
- **MOSAIC**: A multi-object spectrograph designed to study large-scale structures, including galaxy clusters and high-redshift galaxies.

Together, these instruments will allow the ELT to make transformative contributions to IMF research. By providing precise brightness and mass measurements, even in heavily crowded and dust-obscured regions, the ELT will enable detailed studies of star formation processes across diverse environments.

1.3.2. MICADO: The ELT's First-Light Camera

The **Multi-AO Imaging Camera for Deep Observations (MICADO)** (Fig. 1.2) is the ELT's first-light near-infrared camera, specifically built to take advantage of the ELT's high-resolution capabilities. MICADO has a pixel scale of 4 milliarcseconds (mas), giving it very fine detail across a 53x53 arcsecond field of view (FoV). This makes MICADO ideal for studying crowded stellar fields, like the centers of star clusters and the Galactic core, where stars are very close together [Davies et al., 2010].

MICADO is equipped with nine detectors, each having 4096×4096 pixels. It works with the ELT's adaptive optics to produce sharp, diffraction-limited images, even with atmospheric turbulence. MICADO is sensitive enough to detect stars as faint as 27.7 mag (Vega) in the J-band and 27.3 mag (Vega) in the K-band when using MCAO [Davies et al., 2010].

The instrument has been designed to fully integrate with the AO laser-guide-star MCAO system provided by the Multi-Conjugate Adaptive Optics Relay (MAORY) consortium. MCAO uses multiple deformable mirrors to correct atmospheric turbulence across different altitudes, ensuring consistent and high-quality imaging over a wider field of view.

In addition to MCAO, MICADO also supports a dedicated SCAO (Single-Conjugate Adaptive Optics) mode. This mode relies on a single natural guide star to provide highly precise corrections within a smaller field of view. When using SCAO, the sensitivity in the J-band improves significantly to approximately 29.5 mag (Vega), while the Ks-band sensitivity remains unchanged [Davies et al., 2021].

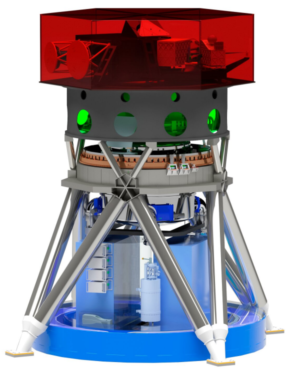

Figure 1.2.: An artist depiction of MICADO: The Multi-AO Imaging Camera for Deep Observations. Image credit: MICADO consortium/ESO

1.3.3. Comparison with NIRCam and HAWK-I

While MICADO offers superior resolution compared to other near-infrared instruments, it is useful to compare its capabilities with those of the **NIRCam** instrument on the **James Webb Space Telescope (JWST)** and the **HAWK-I** instrument on the Very Large Telescope (VLT). Table 1.1 summarizes the differences in the features of the three instruments. It is important to note that the limiting magnitudes listed for MICADO are based on its operation with MCAO. When operating with SCAO, the sensitivity in the J-band improves to approximately 29.5 mag (Vega), while the Ks-band sensitivity remains unchanged.

- **JWST's NIRCam**: JWST's Near-Infrared Camera (NIRCam) operates in a similar wavelength range as MICADO but is optimized for space-based observations. NIRCam provides an FoV of 2.2x2.2 arcminutes with a pixel scale of 31 mas [Rieke et al., 2005]. JWST's space-based platform offers two main benefits: the elimination of atmospheric background emission and an ultra-stable point spread function (PSF) due to the absence of atmospheric turbulence. However, it has a lower resolution compared to MICADO's 4 mas pixel scale. While JWST excels in wide-field imaging and deep field observations, making it ideal for surveying large areas of the sky, it has less ability to resolve crowded fields as finely as MICADO.
- **HAWK-I**: HAWK-I is a ground-based near-infrared camera on the VLT that operates with a pixel scale of 106 mas and covers a large FoV of 7.5 x 7.5 arcminutes [Kissler-Patig et al., 2008]. While HAWK-I offers a significantly larger FoV than MICADO, its lower resolution has historically limited its ability to resolve stars in extremely crowded regions, as it initially operated without adaptive optics (AO). However, HAWK-I now benefits from AO through the ESO Adaptive Optics Facility (AOF) on UT4. This system uses Ground-Layer AO, achieving an FWHM of 0.2-0.3", which enhances its resolving power compared to earlier configurations. Despite this improvement, its resolution still falls short of MICADO's capabilities. The light in HAWK-I's optical path passes through four mirrors and two filter wheels before reaching a mosaic of four Hawaii 2RG detectors, each with 2048 x 2048 pixels, allowing it to capture wide-field images in the near-infrared.

In summary, MICADO's combination of high resolution, small pixel scale, and adaptive optics make it uniquely suited for studies of dense stellar environments. While JWST and HAWK-I are powerful instruments for wide-field surveys and deep-field imaging, MICADO's ability to resolve individual stars in crowded fields will be crucial for studying the IMF, especially in the dense central regions of young star clusters.

Feature	**MICADO (ELT)**	**NIRCam (JWST)**	**HAWK-I (VLT)**
Telescope Diameter	39 m	6.5 m	8 m
Wavelength Range	0.8–2.4 μm	0.6–5.0 μm	0.9–2.5 μm
Pixel Scale	4 mas/pixel	31 mas/pixel	106 mas/pixel
Field of View	53 x 53 arcsec	2.2 x 2.2 arcmin	7.5 x 7.5 arcmin
Limiting Mag. Vega (J)	27.7 mag	27.9 mag (F115W)	23.9 mag
Limiting Mag. Vega (Ks)	27.3 mag	27.3 mag (F200W)	22.3 mag
Specific Crowding Limit	8 px	6 px	10 px

Table 1.1.: Comparison of MICADO, NIRCam, and HAWK-I Instrument Characteristics

2. Methods

This chapter provides an overview of the methods employed in this project to study the Initial Mass Function (IMF) of open star clusters using simulated data. The workflow is broadly divided into four main stages: data preparation, modeling, simulation, and photometric analysis. Each stage contributes to building realistic star cluster models and simulating observations, which are then used to assess the detectability of stars in crowded fields.

- **Data Preparation:** The Milky Way Star Cluster (MWSC) catalogue [MWSC, 2013] was used as the primary dataset, supplemented with tidal masses from the recent study of [Just et al., 2023]. A filtering process was applied to create a subset of open clusters observable with the Extremely Large Telescope (ELT) and containing at least 100 stars within MICADO's field of view.
- **Modelling Star Clusters:** The spatial distribution of stars in each cluster was modeled using the King profile [King, 1962], while the Kroupa IMF [Kroupa, 2001] was employed to generate stellar masses. Stellar positions, masses, and magnitudes were computed and stored in an astropy table.
- **Simulations:** The ScopeSim astronomical simulator [Leschinski et al., 2020] was used to generate realistic observations as they would be seen by the MICADO instrument on the ELT. These simulations incorporated specific instrument parameters, such as pixel scale and detector configuration, as well as exposure times. The output data, including FITS files for both J and Ks bands, provided mock observations for subsequent photometric analysis.
- **Analysis:** The simulated data was processed to perform photometric analysis, focusing on extracting the flux and signal-to-noise ratios for stars within the field of view. The properties of each cluster were analyzed to assess the feasibility of future observations focusing on the IMF.

The following sections will expand on each of these methods in detail, outlining the specific procedures and tools used at each stage of the research process.

2.1. Data preparation

The open star cluster table for this research project was compiled through a series of steps, each contributing to the comprehensive understanding of open star clusters in the Milky Way:

2.1.1. Initial Data Collection from MWSC Catalogue

The Milky Way Star Cluster catalogue [MWSC, 2013] serves as the primary source for the initial dataset. It offers an extensive compilation of open star clusters along with various astrophysical parameters [Kharchenko et al., 2013].

From the MWSC data columns including the MWSC number (unique identifier for each cluster), cluster name, right ascension (RA), declination (DEC), log age (yrs), distance (in pc), and the three King parameters: core radius (r_c), tidal radius (r_t), and central surface density (σ_0) were extracted.

2.1.2. Tidal Mass Acquisition

The MWSC catalogue does not include cluster masses, which are essential for studying the IMF and understanding the overall mass distribution within star clusters. To address this, the tidal masses for the clusters were obtained from the study "Global survey of star clusters in the Milky Way VII. Tidal parameters and mass function" by [Just et al., 2023]. Tidal mass refers to the total mass contained within a star cluster's tidal radius, which marks the outer boundary where the gravitational influence of the cluster is balanced by external forces, such as the gravitational field of the Milky Way.

The relevant data was downloaded from the CDS Astronomy & Astrophysics database [CDS, 2023] and was merged by MWSC number with the previously compiled cluster catalogue.

2.1.3. Other Features of the Table

- **Conversion from equatorial to galactic coordinates:** The right ascension (RA) and declination (DEC) were converted to galactic coordinates (Galactic longitude l and latitude b) for each cluster using `astropy.coordinates` [Astropy, 2013]. This transformation was necessary to analyze the spatial distribution of clusters within the Milky Way's galactic frame, which is more suitable for studying their positions relative to the galactic center. Using galactic coordinates also simplifies observation planning with instruments like MICADO.

- **Core Radius in Arcseconds:** The core radius of each cluster was calculated in arcseconds to provide a clearer visualization of the core size relative to observational capabilities, using equation 2.1:

$$\text{core radius (arcsec)} = \frac{\text{core radius (pc)}}{\text{distance (pc)}} \times 206265. \tag{2.1}$$

  The factor 206265 originates from the small-angle approximation, where $\tan(x) \approx x$ for small angles measured in radians. This approximation is almost always true in astronomy due to the large distances involved. Since 1 radian corresponds to 206265 arcseconds, the formula provides a convenient way to convert linear sizes in parsecs to angular sizes observable from Earth [Binney and Merrifield, 1998].

This conversion is essential for comparing the cluster's core radius to the angular resolution of instruments like MICADO.

- **Number of Stars in Tidal and Core Radius:** The number of stars within the tidal radius as well as the core radius was estimated by simulating star positions using the King profile parameters and counting the number of stars that fall within each radius in parsecs. This information is crucial for understanding the stellar density within different regions of the cluster, which directly impacts crowding and photometric completeness in observational studies.

- **Number of Stars in MICADO's FOV:** The number of stars within MICADO's field of view on the ELT was calculated to provide insight into the potential observational data quality for each cluster. This helps assess whether the selected clusters have sufficient stellar populations to allow for meaningful IMF studies while remaining manageable in terms of crowding effects.

- **Number of Stars in MICADO's Central Detector:** The number of stars within MICADO's central detector, which has a field of view of approximately 17.8x17.8 arcseconds, was calculated for each cluster. This is important because the stellar density in the central detector is significantly higher than the average density within the core radius, making it critical to evaluate crowding effects and their implications for high-resolution photometry.

- **Number of MICADO Fields of View based on Core Radius and Tidal Radius:** The number of MICADO fields required to cover the core and tidal radii of each cluster was calculated to estimate the observational effort needed for complete spatial coverage. This calculation ensures that sufficient observations are planned to fully resolve the stellar populations within the cluster's core and tidal regions.

$$\text{num\_fields} = \left(\frac{\text{radius (arcsec)}}{\text{MICADO FOV (arcsec)}}\right)^2 \tag{2.2}$$

  Equation 2.2 is derived by dividing the area of the region (core or tidal radius) by the area of MICADO's field of view, assuming a square geometry for simplicity. Since MICADO's FOV is 53x53 arcseconds, this method provides a straightforward estimate of how many pointings are needed for full coverage.

- **Star Density in Tidal Radius Area and Core Radius Area:** The star density within the tidal radius as well as within the core radius was calculated to quantify the stellar density in these regions. This is essential for assessing crowding effects and evaluating the feasibility of accurate photometric measurements within each region.

$$\text{star density (stars/arcsec}^2\text{)} = \frac{\text{number of stars}}{\pi \times (\text{radius (arcsec)})^2} \tag{2.3}$$

Equation 2.3 is derived from the definition of surface density, where the area of a circular region is πr^2. These densities are particularly important for understanding observational challenges such as crowding effects for studies of the IMF.

- **Pixels Per Star for MICADO, NIRCam, and HAWK-I:** The number of pixels per star in the field of view was calculated for each instrument to assess the extent of crowding in the science images. Crowding directly affects the ability to reliably measure the flux and position of individual stars.

$$\text{pixels\_per\_star} = \frac{\text{FOV} \times \text{pixel scale}}{\text{number of stars}} \tag{2.4}$$

  This metric indicates how many pixels are available per star in the image, providing insight into how well-resolved individual stars will be and how much contamination may occur due to overlapping PSFs.

  The pixel scales used for the calculations were:

  - MICADO: 4 mas/px [Davies et al., 2010]
  - NIRCam: 31 mas/px [Rieke et al., 2005]
  - HAWK-I: 106 mas/px [Kissler-Patig et al., 2008]

- **Crowding Distance for MICADO, JWST, and HAWK-I:** The crowding distance, which represents the average angular separation between stars, was calculated for each instrument (MICADO, NIRCam and HAWK-I).

$$\text{crowding\_distance} = \sqrt{\text{pixels\_per\_star}} \tag{2.5}$$

  Equation 2.5 originates from the assumption that stars are evenly distributed across the field of view. The area per star, given by pixels_per_star, is treated as approximately circular, and its square root provides the average distance between neighboring stars. This distance is a critical parameter for understanding the level of blending in crowded fields.

  Calculating the crowding distance helps evaluate whether individual stars can be resolved in dense environments by a certain instrument, particularly in regions like the Galactic center, where crowding is a significant challenge for IMF studies.

2.1.4. Filtering the Cluster Sample

The initial dataset from the MWSC catalogue, contained a total of 2826 open clusters. To create a final sample suitable for high-resolution study with MICADO and observable with the ELT, a series of filtering criteria was applied:

1. **Observability by ELT**: Clusters were first evaluated based on their declination to determine if they fall within the ELT's observable range. This range is determined

by the ELT's location at Cerro Armazones in Chile, with coordinates latitude $-24.6°$ and longitude $-70.2°$ [European Southern Observatory (ESO), 2024]. The observability range is calculated based on the latitude, covering latitude $\pm55°$, allowing the telescope to view declinations from $-79.6°$ to $+30.4°$.

2. **Number of Stars in MICADO's FOV:** Clusters were then filtered to include only those with at least 100 stars within MICADO's field of view (53x53 arcseconds), based on simulated stellar distributions.

By applying these filters, the initial dataset was reduced to a final sample of **1047 open clusters**, which are well-suited for further observational studies with the ELT and MICADO.

2.2. Modelling Star Clusters

The Python code used for implementing the modeling of star clusters, including the generation of stellar masses, is provided in Appendix A.1.1 for reference.

2.2.1. Initial Mass Function (IMF) Implementation

In this project, the Kroupa IMF [Kroupa, 2001] was exclusively used to model the mass distribution of stars within simulated star clusters. The Kroupa IMF is well-suited for modeling stellar populations in the Milky Way, but it is important to remember that the true nature of the IMF is still unknown.

The `IMF` Python package [Ginsburg, nd] was employed to generate the stellar masses according to the Kroupa IMF. This package allows for the sampling of stellar masses that follow the prescribed IMF, ensuring that the distribution is consistent with observational data. While the package offers options to use other IMFs, such as Salpeter and Chabrier, only the Kroupa IMF was used for the simulations in this study. Fig. 2.1 is the modeled stellar mass distribution of an example cluster, in this case Berkeley 85.

2.2.2. King Profile for Spatial Distribution

The King model [King, 1962] is widely used to describe the spatial distribution of stars in a star cluster. It assumes a spherically symmetric distribution with a dense central core and a defined tidal radius, beyond which stars are no longer gravitationally bound to the cluster. The King profile was implemented to generate the positions of stars within the core and tidal radii of modeled clusters, providing a realistic representation of the structure of open star clusters by capturing both the dense core and the more diffuse outer regions.

The surface density of stars as a function of radial distance, r, from the cluster center is given by the King profile equation:

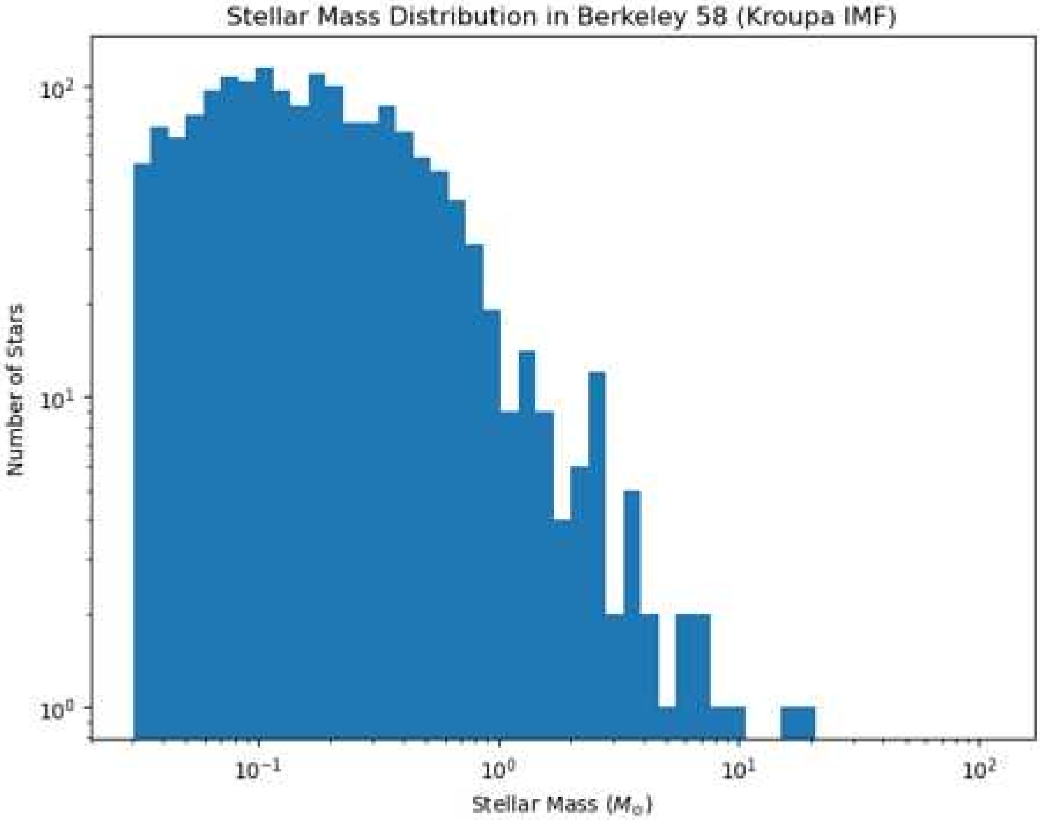

Figure 2.1.: The three-segment structure of the Kroupa Initial Mass Function (IMF) is visible in the stellar mass distribution plot of the cluster Berkeley 85.

$$\sigma(r) = \sigma_0 \left[\frac{1}{\sqrt{1+\left(\frac{r}{r_c}\right)^2}} - \frac{1}{\sqrt{1+\left(\frac{r_t}{r_c}\right)^2}} \right]^2 \tag{2.6}$$

where:

- $\sigma(r)$ is the surface density at distance r,
- σ_0 is the central surface density,
- r_c is the core radius,
- r_t is the tidal radius.

Star positions were generated using this profile and then converted from parsecs to arcseconds to match the observational frame. This conversion allowed for direct comparisons with the field of view of instruments like MICADO, JWST, and HAWK-I. The simulated stellar positions of Berkeley 58, based on the King profile, are shown in Figure 2.2.

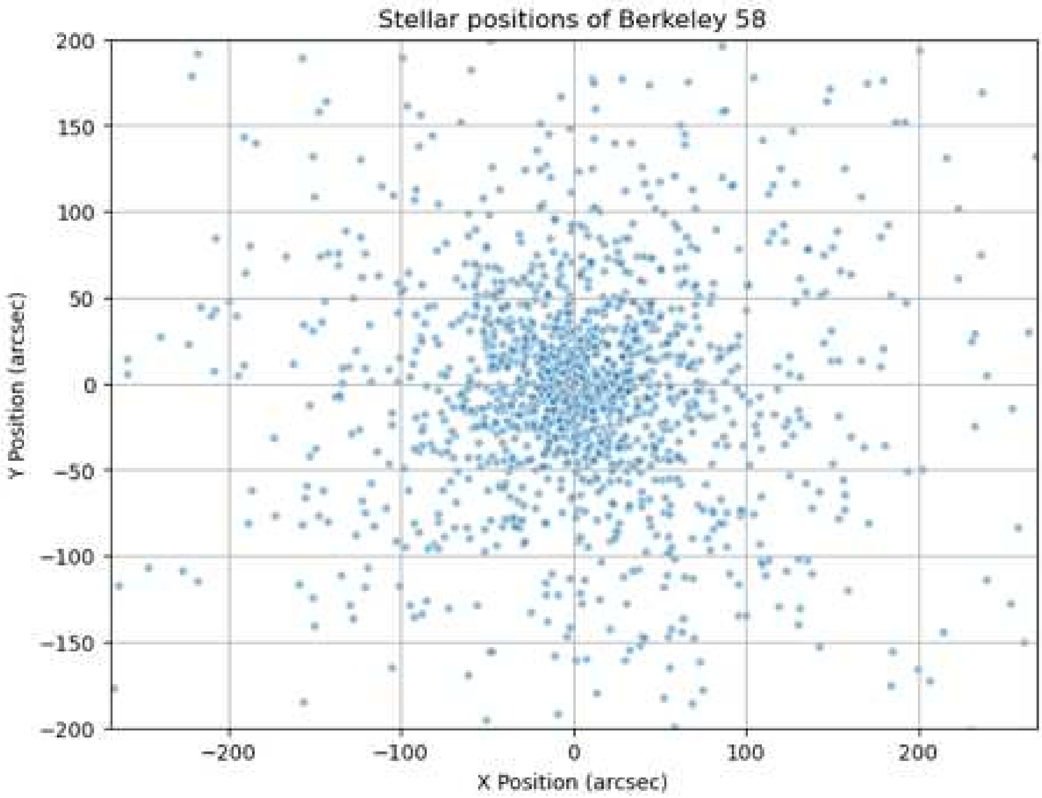

Figure 2.2.: Stellar positions of Berkeley 58, simulated using the King profile. The plot shows the X and Y positions of stars in arcseconds relative to the cluster center.

2.2.3. Apparent magnitudes and spectral types

To derive realistic J-band and Ks-band magnitudes for stars in the cluster models, stellar masses were mapped to magnitudes using empirical data from Eric Mamajek's table [Mamajek, 2013]. This table provides a comprehensive set of stellar parameters for various spectral types, spanning a wide range of masses.

First, linear interpolation was used to estimate J and Ks absolute magnitudes for stellar masses that did not directly correspond to values in the table. For stellar masses outside the available range, the nearest valid magnitude was used to avoid extrapolation.

The interpolated absolute magnitudes were then converted to apparent magnitudes based on the distance to the cluster, using the standard formula:

$$m = M + 5\log_{10}(d) - 5 \tag{2.7}$$

where:

- m is the apparent magnitude,
- M is the absolute magnitude,
- d is the distance to the cluster in parsecs.

This formula is derived from the distance modulus, a standard relation in observational astronomy [Binney and Merrifield, 1998].

Finally, spectral types were assigned to stars based on their masses using the `mass2spt` function from the `scopesim_templates.stellar` [Vienna,] package. This function provided a mapping from stellar mass to spectral type, ensuring that each star in the simulated cluster had a realistic spectral classification.

2.2.4. Age-Based Filtering of Stars

In addition to assigning masses, magnitudes, and positions to the stars in the simulated clusters, a filter was applied to remove stars that are inconsistent with the cluster's age. Based on the logarithmic age (`log_age`) of each cluster, stars of certain spectral types were excluded, ensuring that the simulation reflects realistic stellar populations for clusters of different ages. The filter was applied as follows:

- For younger clusters with $\log(\text{age}) < 7.0$, all spectral types were included.
- For clusters with $7.0 \leq \log(\text{age}) < 8.0$, the most massive O-type stars were removed, leaving stars of types B, A, F, G, K, and M.
- For clusters with $8.0 \leq \log(\text{age}) < 9.0$, B-type stars were also removed.
- For clusters with $\log(\text{age}) \geq 9.0$, only lower-mass stars of types F, G, K, and M were retained.

This filtering process ensures that older clusters, which have lost their massive O- and B-type stars due to stellar evolution, are represented more accurately in the simulations.

The filtering approach was based on stellar evolution models, which show that massive stars have short lifetimes (on the order of millions of years), while lower-mass stars (F, G, K, and M-types) have much longer lifetimes, extending to billions or even trillions of years. The stellar population synthesis models from Bruzual and Charlot (2003) [Bruzual and Charlot, 2003] were used as a reference for the stellar lifetimes employed in this filtering process.

2.2.5. Simulation Parameters

To generate realistic star clusters, only these key parameters were used:

- **Total Cluster Mass:** Stellar masses were generated using the Kroupa IMF and normalized to match the total cluster mass.
- **Core and Tidal Radii:** The King profile was applied to simulate the spatial distribution of stars, using the core radius (r_c) and tidal radius (r_t) for each cluster, both extracted from the MWSC catalogue. These radii define the central concentration and the outer boundary of the cluster.
- **Cluster Distance:** The distances to each cluster, also provided by the MWSC catalogue, were used to convert absolute magnitudes to apparent magnitudes for both the J and Ks bands.

The output data, including star positions, magnitudes, masses, and spectral types, were organized into an Astropy table. This table forms the basis for further analysis and simulation with ScopeSim A.1.1.

2.3. Simulation

The primary goal of the simulation stage was to generate mock observations of open star clusters using the MICADO instrument on the Extremely Large Telescope (ELT). These simulations aimed to reproduce realistic conditions that will be encountered during actual observations, allowing for a detailed analysis of the observational feasibility of resolving stars and studying the Initial Mass Function (IMF) in crowded stellar fields. The Python code used to set up and run these simulations is described in detail in Appendix A.1.2.

2.3.1. ScopeSim Setup

Simulations were carried out using the `ScopeSim` toolkit [Leschinski et al., 2020], a flexible framework for simulating astronomical observations with various instruments, including MICADO. While the full field of view (FoV) of MICADO is 53x53 arcseconds, the simulation was performed using only the central detector, which covers 4096x4096 pixels. This smaller area was sufficient for resolving stars in dense regions while maintaining a high spatial resolution. ScopeSim allows for detailed configuration of key instrument settings, such as pixel scale, field of view, exposure time, and observational filters.

For this project, the following key instrument settings were used in ScopeSim to simulate observations with MICADO:

- **Field of View (FoV):** The simulation was done using the central detector with 4096x4096 pixels.

- **Pixel Scale:** 4 milliarcseconds per pixel, providing the high spatial resolution necessary to resolve stars in crowded fields.

- **Filters:** Simulations were conducted in both the J-band and Ks-band, corresponding to the near-infrared sensitivity of MICADO.

- **Exposure Time:** A single exposure time of 60 seconds (DIT = 60) was used, with a total of 60 stacked exposures (NDIT = 60) for each observation. This consists of a total observation time of 1 hour per filter, which is realistic considering the high demand for future ELT observing time.

These settings were chosen to reflect realistic observational conditions for studying star clusters, taking into account MICADO's high spatial resolution and sensitivity in the near-infrared range.

2.3.2. Cluster Simulation Input

The stellar properties, including positions and apparent magnitudes in both the J and Ks bands, were generated in the earlier steps and stored in an Astropy table. These apparent magnitudes served as the key input for the simulation process, ensuring that each star was modeled with a realistic brightness level. Specifically:

- **Stellar Positions:** Star positions were generated using the King profile for the spatial distribution, ensuring a realistic representation of both the dense core and outer regions of the cluster.

- **Apparent Magnitudes:** Apparent magnitudes in the J-band and Ks-band were derived from interpolating stellar masses and then converting absolute magnitudes into apparent magnitudes based on the cluster distance.

- **Spectral Types:** Spectral types were assigned based on stellar mass using the `mass2spt` function from the `scopesim_templates.stellar` package.

2.3.3. Simulating Observations

Simulations were automatically run for all 1049 clusters in the final cluster catalogue. For each cluster, ScopeSim generated mock observations in both the J and Ks bands, producing FITS files as the output. These FITS files contained the flux values of all pixels in the field of view. Details of the Python code used for these simulations, including the setup of ScopeSim and the parameters used, are provided in Appendix A.1.2.

The main focus of these simulations was to study the detectability of stars within the cluster, particularly those at the low-mass end of the IMF. The FITS files generated from these simulations will serve as the foundation for further analysis, where the detectability of stars and observational challenges in crowded regions will be explored.

2.4. Photometric Analysis

Photometric analysis was performed on the simulated data generated from the ScopeSim observations to evaluate the detectability of stars in the star clusters. This analysis focused on extracting flux values and signal-to-noise ratios (SNR) using rectangular aperture photometry. Details of the Python code used for the photometric analysis are provided in Appendix A.1.3.

2.4.1. Aperture Photometry

Rectangular aperture photometry was used, employing three different aperture sizes: ap0, ap1, and ap2, with values of 7, 20, and 30 pixels, respectively. The known x, y positions of stars were used to center these apertures, bypassing the need for star-finding algorithms like DAOStarFinder (more in the discussion chapter 4). The procedure involved the following steps:

- **Aperture Definition:** Rectangular apertures with sizes of 7, 20, and 30 pixels were placed at the x, y positions of each star.
- **Background Subtraction:** Local background levels were measured at the largest aperture to subtract any contribution from the sky background.
- **Flux Measurement:** The total flux within each aperture was calculated in both the J and Ks bands, providing photometric brightness estimates for the stars.

As an example, the image 2.3 shows the photometric measurement of a star with spectral type M4.5V and a signal-to-noise ratio (SNR) of 229. The red, yellow, and blue boxes correspond to the three aperture sizes (ap0 = 7, ap1 = 20, ap2 = 30), used to measure the flux of the star and the background noise.

2.4.2. Signal-to-Noise Ratio (SNR)

For each star, the signal-to-noise ratio (SNR) was computed based on the measured flux, background noise, and readout noise from the MICADO instrument. The SNR was calculated using equation 2.8 [Hainaut, 2005].

$$SNR = \frac{F}{\sqrt{F + N_{\text{bg}} + RON}} \tag{2.8}$$

where:

- F is the measured flux,
- N_{bg} is the background noise contribution,
- RON is the readout noise from the instrument, set to 10 electrons.

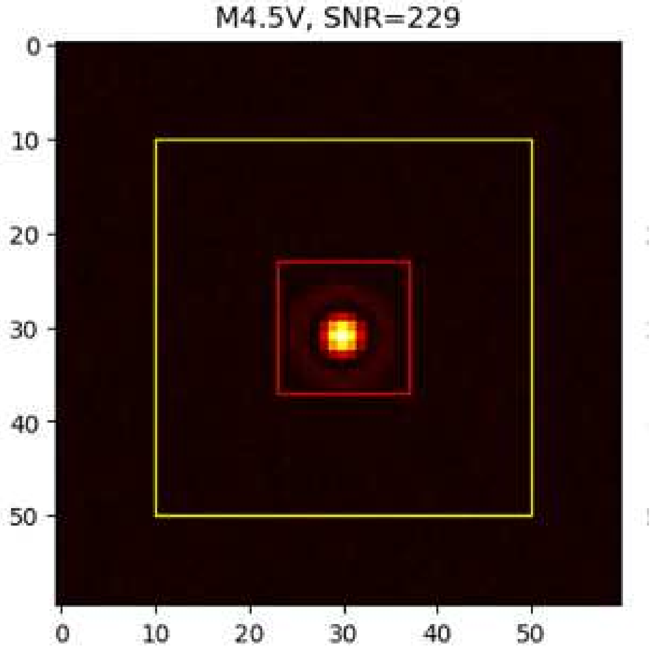

Figure 2.3.: Example of aperture photometry for an M4.5V star.

2.4.3. Output Data

For all 1049 clusters, the final output table from the photometric analysis contains the following parameters for each star:

- Mass
- J Magnitude (absolute and apparent)
- Ks Magnitude (absolute and apparent)
- X and Y Positions (in parsecs and arcseconds)
- Spectral Type
- Flux in J and Ks bands
- SNR in J and Ks bands

The photometric analysis produced a detailed dataset of stellar fluxes and signal-to-noise ratios (SNR), which will serve as the foundation for evaluating the detectability of stars within crowded regions of the simulated clusters. These results provide a solid basis for assessing the success of the MICADO simulations and the observational reliability of the data.

With this, the simulation pipeline is complete. Stellar properties, spatial distributions, and magnitudes are now linked with simulated observations. This setup allows exploration of observational challenges, like crowding, in studies of dense star clusters.

The outcomes of this dataset will be examined in the upcoming chapter 3, which will offer valuable information on the simulation's efficacy and the detectability boundaries in crowded fields.

3. Results

3.1. Overview of Cluster Properties in the Final Table

The final table (description of all parameters: Table 3.1) is available on GitHub at `https://github.com/MaxiKoe/IMF_MasterProject`. It's a FITS file which includes a comprehensive set of astrophysical parameters for each of the 1049 cluster, combining data from the MWSC catalogue, tidal masses, King profile parameters, and additional calculated fields.

These properties give a detailed view of each open cluster, making the final table essential for theoretical studies and simulations. The mix of observational data, theoretical parameters, and calculated fields provides a strong foundation for studying the Initial Mass Function in open clusters, especially for future ELT and MICADO observations.

Parameter	Description
SOURCE_NUMBER	A unique identifier for each cluster from the MWSC catalogue.
NAME	The name of the open cluster.
TIDAL_MASS	The total mass inside the tidal radius of the cluster.
DISTANCE	The distance to the cluster in parsecs (pc).
LOG_AGE	The logarithmic age of the cluster in years.
RA and DEC	The equatorial coordinates Right Ascension (RA) and Declination (DEC) of the cluster.
GAL_LON and GAL_LAT	The Galactic coordinates, Galactic longitude (l) and latitude (b), for spatial mapping in the Milky Way.
KING_CORE_RADIUS	The core radius of the cluster in parsecs (pc), a parameter of the King profile.
KING_TIDAL_RADIUS	The tidal radius of the cluster in parsecs (pc), a parameter of the King profile.
KING_NORM_FACTOR	Normalization factor used in fitting the King profile.
KING_CORE_RADIUS_ARCSEC	The core radius of the cluster in arcseconds.
KING_TIDAL_RADIUS_ARCSEC	The tidal radius of the cluster in arcseconds.
MAG_J_G2	The apparent J-band magnitude for a G2 star in the cluster.
MAG_Ks_G2	The apparent Ks-band magnitude for a G2 star in the cluster.
MAG_J_M9	The apparent J-band magnitude for a M9 star in the cluster.
MAG_Ks_M9	The apparent Ks-band magnitude for a M9 star in the cluster.
NUM_STARS_CORE	The estimated number of stars within the core radius.
NUM_STARS_TIDAL	The estimated number of stars within the tidal radius.
NUM_STARS_MICADO	The estimated number of stars within MICADO's FoV.
NUM_STARS_CENTRALDETECTOR	The number of stars expected to fall within MICADO's smaller central detector (17.8x17.8 arcseconds).
STAR_DENSITY_CORE	The calculated stellar density ($stars/arcsec^2$) within the core radius.
STAR_DENSITY_TIDAL	The calculated stellar density ($stars/arcsec^2$) within the tidal radius.
STAR_DENSITY_CENTRALDETECTOR	The calculated stellar density ($stars/arcsec^2$) within the area of MICADO's central detector.
PIXELS_PER_STAR_MICADO	The number of pixels per star within MICADO's 53x53 arcsec field of view.
PIXELS_PER_STAR_JWST	The number of pixels per star within JWST's field of view.
PIXELS_PER_STAR_HAWKI	The number of pixels per star within HAWK-I's field of view.
CROWDING_DISTANCE_MICADO	The average distance between stars in MICADO's FoV.
CROWDING_DISTANCE_JWST	The average distance between stars in JWST's FoV.
CROWDING_DISTANCE_HAWKI	The average distance between stars in HAWK-I's FoV.
NUM_MICADO_FIELDS_CORE	The calculated number of MICADO fields of view required to fully observe all stars in the core radius of the cluster.
NUM_MICADO_FIELDS_TIDAL	The calculated number of MICADO fields of view required to fully observe all stars in the tidal radius of the cluster.

Table 3.1.: Description of the parameters in the final cluster dataset

3.2. Global Statistics of the Data Set

The following section provides an overview of key properties of the open star clusters in the final dataset. Various statistical plots have been generated to illustrate the distribution of cluster parameters such as distance, mass, age, and structural characteristics.

The first histogram (Figure 3.1) shows the number of clusters as a function of distance. The majority of clusters in the dataset are located within a range of 1,000 to 5,000 parsecs, with the distribution showing a sharp drop-off at larger distances. Open clusters, being young stellar objects, are typically associated with the Galactic spiral arms where star formation is most active. The Sun's position between two spiral arms results in most observable clusters being located within nearby arms, while clusters on the far side of the Galaxy are obscured by the Galactic bulge and interstellar extinction. Some of the clusters have greater distances though, with *Saurer 1* being the most distant cluster at 13,700 pc. In reality the Milky Way should have clusters distributed equally throughout the whole disk.

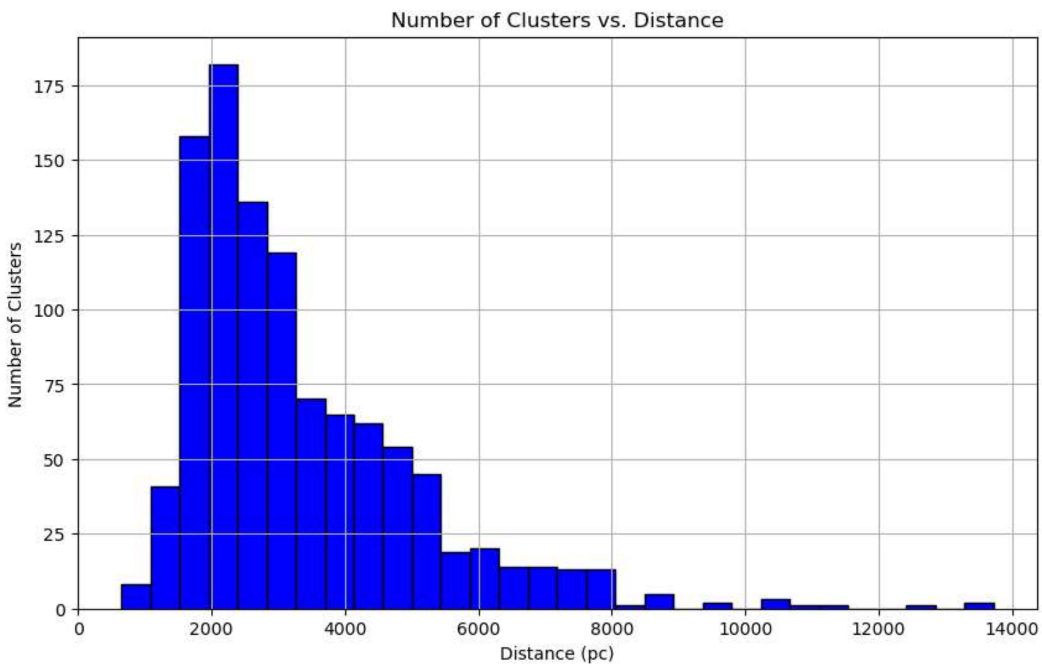

Figure 3.1.: Number of Clusters vs. Distance. The majority of clusters are located within 1,000–5,000 pc, reflecting their association with nearby Galactic spiral arms and the effects of observational limitations such as interstellar extinction and the obscuration by the Galactic bulge.

A second histogram (Figure 3.2) focuses on the distribution of cluster masses, presented on a logarithmic scale. This representation captures the wide range of masses present in the dataset. The majority of clusters have masses between 300 and 1000 $M_{\odot}$, which is typical for open star clusters in the Milky Way, where low-mass clusters are more common than high-mass ones. However, a few clusters have much higher masses, reaching up to 300,000 $M_{\odot}$. The most massive cluster in the dataset is *vdBergh-Hagen 222*.

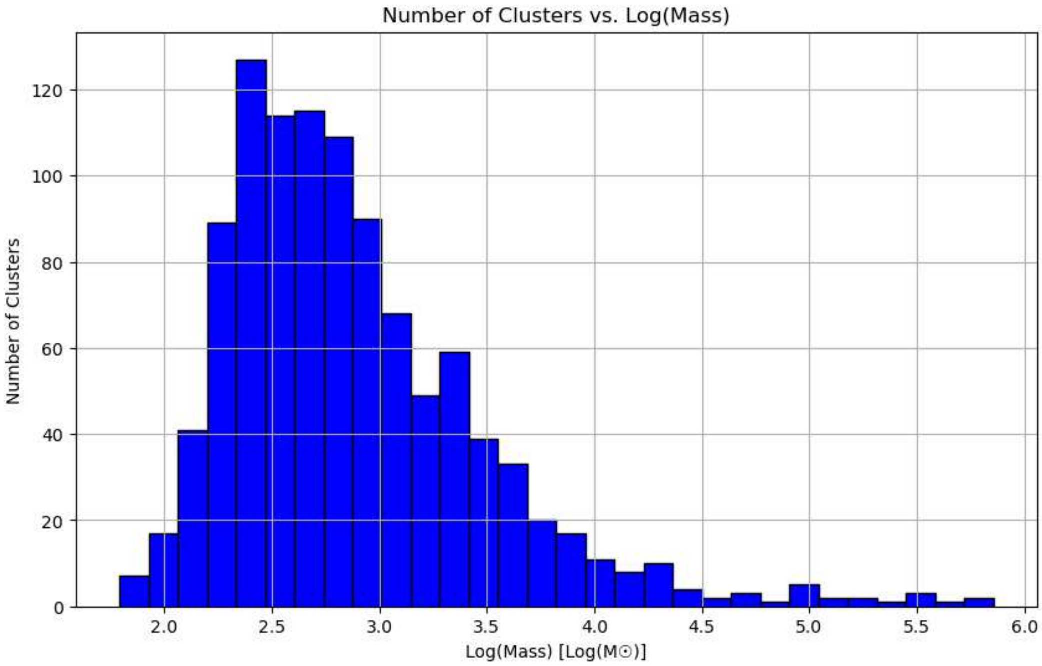

Figure 3.2.: Number of clusters as a function of Log(Mass). The histogram highlights the dominance of low-mass clusters in the dataset, typical for open clusters in the Milky Way, while a few high-mass clusters extend the distribution up to 300,000 $M_{\odot}$.

The age distribution is visualized in another histogram (Figure 3.3), which shows that clusters in the dataset cover a broad range of ages, from a few million years to several billion years. Most of the clusters are older, with the most common age in the dataset being approximately 1 billion years. Younger clusters, on the other hand, still contain massive stars, such as O and B types, which have short lifetimes. As clusters age, these massive stars evolve or explode as supernovae, leaving behind lower-mass, long-lived stars in older clusters.

In this study, the focus is on the lower-mass end of the IMF, as the high-mass end is already well understood. Although older clusters lack high-mass stars due to stellar evolution, they still provide valuable insight into the low-mass end of the IMF.

A scatter plot (Figure 3.4) was created to show the relationship between core radius and tidal radius for all clusters, presented on a log-log scale for better visualization. A

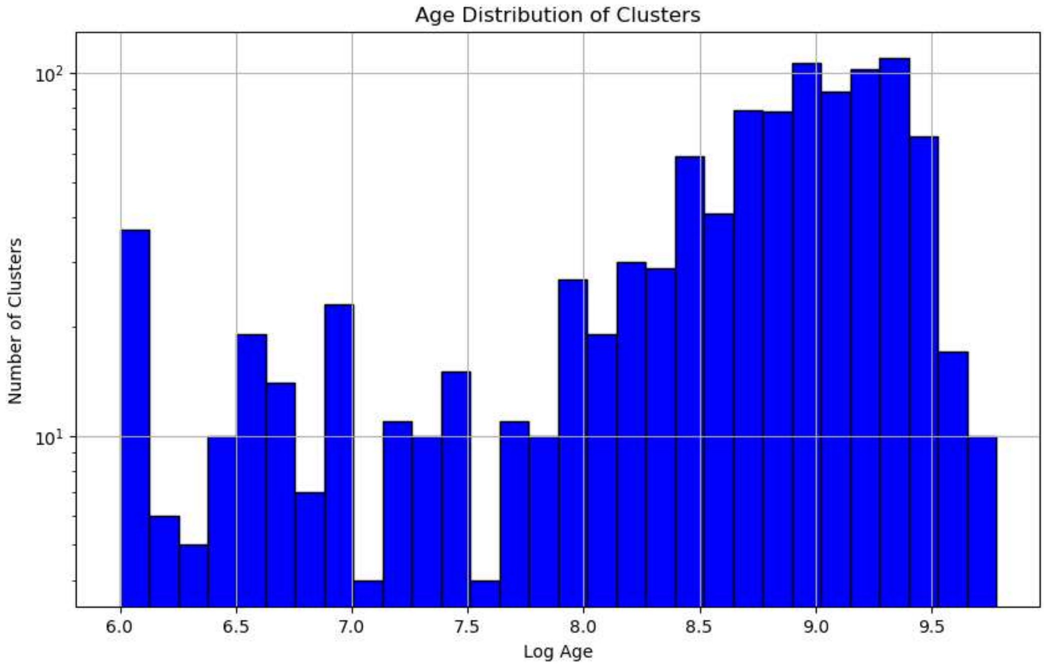

Figure 3.3.: Age Distribution of Clusters. While older clusters no longer contain high-mass stars due to stellar evolution, they remain valuable for this study as they provide insights into the low-mass end of the IMF.

clear trend is visible, showing that clusters with larger core radii generally have larger tidal radii, although the scattering in the data is still substantial. Most clusters tend to have relatively small core radii (below 5 parsecs), while tidal radii vary more significantly, with a few outliers having tidal radii greater than 40 parsecs.

This plot highlights the structural differences among the clusters. While some clusters have a relatively small and compact area, others exhibit such large tidal radii that observing them entirely with MICADO will be challenging. The largest cluster in the dataset is *vdBergh-Hagen 79*, with a tidal radius of 57 pc (or angular size of 1150 arcsec).

The number of MICADO fields required to observe the entire cluster (both core and tidal radius) was also calculated. Most clusters require fewer than 10 MICADO fields to fully cover their core radius (Figure 3.5), while some larger clusters demand up to several hundred fields to cover their tidal radius (Figure 3.6). An example: to observe the whole tidal radius are of the small cluster *DBSB 162* we would need already 13 MICADO fields. On the other hand for the massive cluster *NGC 6494* an overwhelming number of 13,900 MICADO fields would be required! These values demonstrate the challenges of observing extended structures like star clusters with high-resolution instruments, where multiple fields of view are necessary for comprehensive coverage.

Additionally, the total number of MICADO fields required for all clusters in the dataset

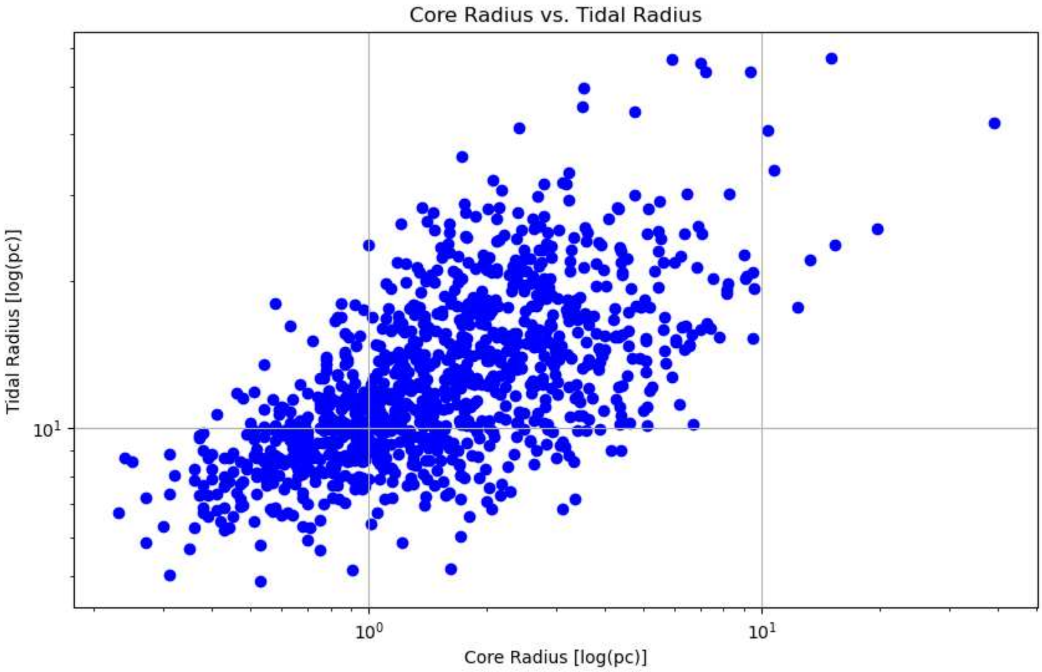

Figure 3.4.: Core Radius vs. Tidal Radius on a log-log scale. A trend towards larger tidal radii with increasing core radii is visible, despite significant scatter. Observing entire clusters with large tidal radii using MICADO will be challenging due to its small field of view.

was calculated to be 385,027. On average, each field requires an observation time of 60 seconds and 60 exposures. Closer clusters generally require less observation time, whereas more distant ones need longer exposures due to their faintness. Taking these factors into account, the total observation time for all fields amounts to approximately 44 years of continuous observing time. This demonstrates the immense challenge of obtaining full coverage for such a large dataset of open star clusters. More about this problem in the Discussion 4 chapter.

In addition, the galactic distribution of clusters was examined using a scatter plot of galactic longitude vs. latitude (Figure 3.7). The majority of clusters are located near the galactic plane, as expected, with a concentration towards the galactic center. This is consistent with the fact that open clusters predominantly form in the spiral arms of the Milky Way, which lie close to the galactic plane. There is a region without clusters in this plot, this is because clusters which are not observable by the ELT were excluded from the dataset.

Star density as a function of distance for all clusters in the dataset is shown in Figure 3.10. Each point represents a cluster, with star density calculated based on the data and

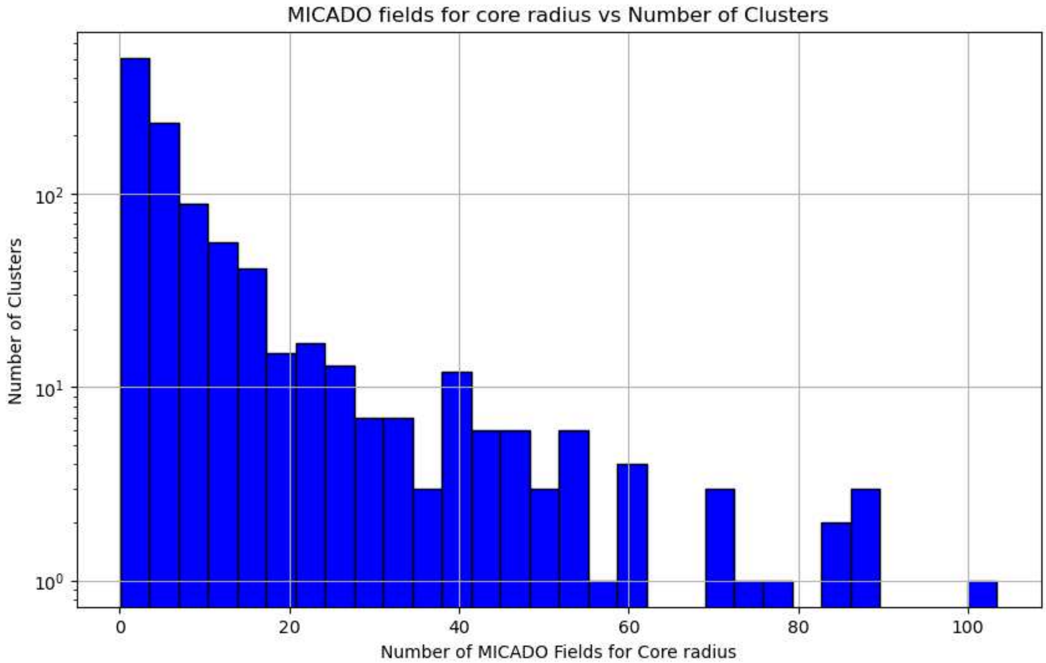

Figure 3.5.: Number of Clusters vs. MICADO Fields for Core Radius. The total number of MICADO fields required to cover all clusters' core radii is 11,511.

plotted against the cluster's distance in parsecs. The points are color-coded according to the core radius of each cluster, with larger core radii shown in yellow and smaller ones in blue, as indicated by the color bar. In general more of the compact clusters can be found on the bottom left of the plot (at lower distances). Clusters with the highest star density are concentrated at around 8 kpc, this is exactly where we find the galactic center.

Threshold lines for MICADO, JWST, and HAWK-I are shown as dashed lines, representing the maximum star density each instrument can effectively handle based on their crowding limits. Calculations suggest that MICADO's crowding threshold (purple) is approximately 1000 stars per arcsec^2, JWST's (orange) at 28 stars per arcsec^2, and HAWK-I's (red) at 2 stars per arcsec^2. These thresholds were derived from each instrument's pixel scale and specific crowding tolerance, defined as 8 pixels for MICADO, 6 pixels for JWST, and 10 pixels for HAWK-I. Clusters exceeding these density thresholds are likely to encounter significant crowding issues, which would complicate individual star detection and photometry. This issue, along with its implications for IMF studies, will be discussed further in chapter 4.

The plots in Figure 3.9 show the relationship between cluster distance and the apparent magnitudes of stars with specific masses, representing key points for the Kroupa IMF and Chabrier IMF. The chosen masses are 0.08 $M_\odot$ (M9 star) - brown dwarfs segment in the Kroupa IMF, 0.2 $M_\odot$ (M4 star) - approximately the characteristic mass of the

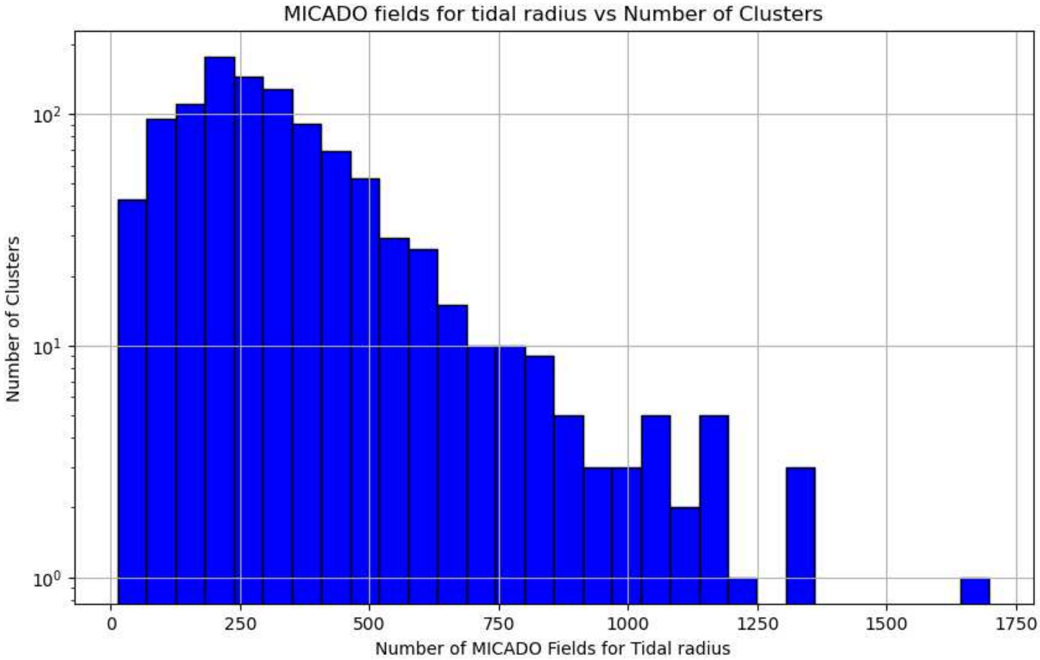

Figure 3.6.: Number of Clusters vs. MICADO Fields for Tidal Radius. The total number of MICADO fields required to cover all clusters' tidal radii is 385,027. This shows the observational challenge of studying entire clusters with large tidal radii using MICADO.

Chabrier IMF, 0.50 $M_\odot$ (K7 star), and 1.00 $M_\odot$ (G2 star, representing the solar mass). These masses cover a range from low-mass stars to solar-mass stars, reflecting both the lower end of the IMF and typical stellar masses.

Each plot includes instrument sensitivity thresholds for MICADO (purple) and HAWK-I (red), allowing us to assess the detectability of stars at various distances for these instruments. The MICADO sensitivity limits (using MCAO) are set at 27.7 mag (J) and 27.3 mag (Ks) for deep observations [Davies et al., 2021]. HAWK-I has comparatively lower limits, with maximum sensitivities of 23.9 mag (J) and 22.3 mag (Ks) in the Vega system [ESO, 2021]. These thresholds are indicated by dashed lines, providing a clear reference for the detectability limits. JWST's NIRCam is not included in these plots as it uses different filters that do not directly correspond to the standard J and Ks bands, making a direct comparison challenging.

In addition, a black dotted horizontal line is included in each plot to indicate the MICADO saturation limit at 15 mag for both J and Ks bands. This saturation limit represents the brightest magnitude above which stars will no longer be measurable without saturating the detector.

The distribution of magnitudes shows that while MICADO can detect stars down to M9 type at all distances up to the edge of the dataset (14,000 pc), HAWK-I's detectability

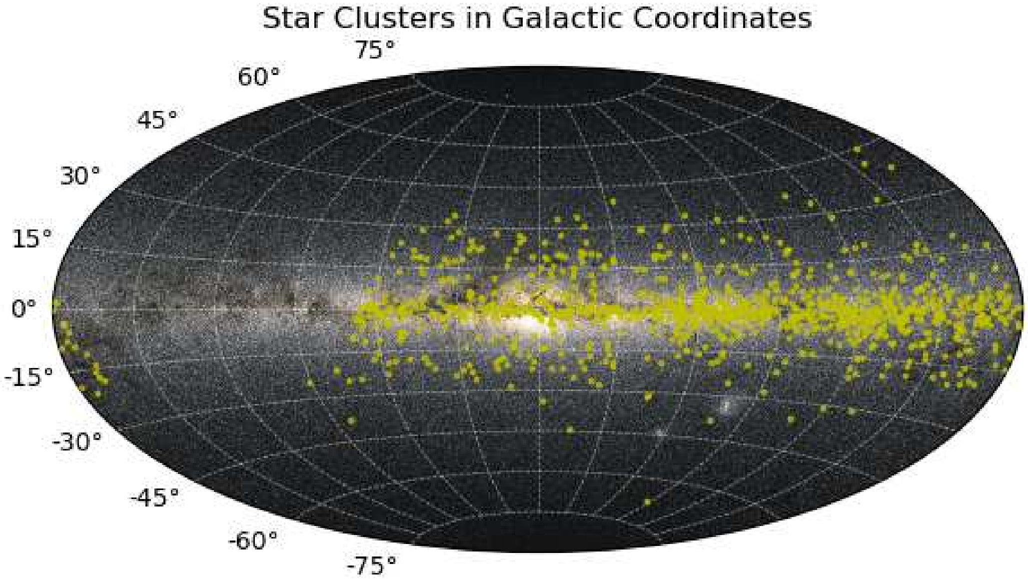

Figure 3.7.: Galactic Distribution of the clusters in the Milky Way. The gap in the distribution reflects the exclusion of clusters that are not observable by the ELT due to it's location.

diminishes beyond certain distances. Specifically, HAWK-I cannot detect M9 stars with a SNR > 5 in the J band beyond approximately 2900 pc and in the Ks band beyond 2400 pc.

These plots highlight the strengths of MICADO in observing faint stars in distant clusters and illustrate the more limited range of HAWK-I. They emphasize the need for the Extremely Large Telescope to detect the full range of spectral types in Milky Way open star clusters and to study the Initial Mass Function in diverse environments, such as the Galactic Center. This is particularly important for gaining a better understanding of the low-mass end of the IMF beyond the solar neighborhood (>2 kpc).

The plots in Figure 3.10 illustrate the relationship between star density in the MICADO central field of each cluster and its distance from Earth. The observational limits of MICADO, JWST, and HAWK-I are shown, with each instrument's effective range highlighted in different crowding-limited zones. For these analyses, distances were calculated based on HAWK-I's apparent magnitude limits for M9V stars, which represent the lower end of the IMF. In the J-band, HAWK-I's limit is 23.9 mag, corresponding to a maximum detection distance of approximately 2900 pc. In the Ks-band, the limit is 22.3 mag, allowing detections up to around 2400 pc. Beyond these distances, HAWK-I struggles to detect low-mass stars with sufficient signal-to-noise ratios.

Each plot is divided into four shaded zones: the green HAWK-I zone, effective for clusters with densities up to 2 stars per arcsec^2 within its detection limit; the red JWST

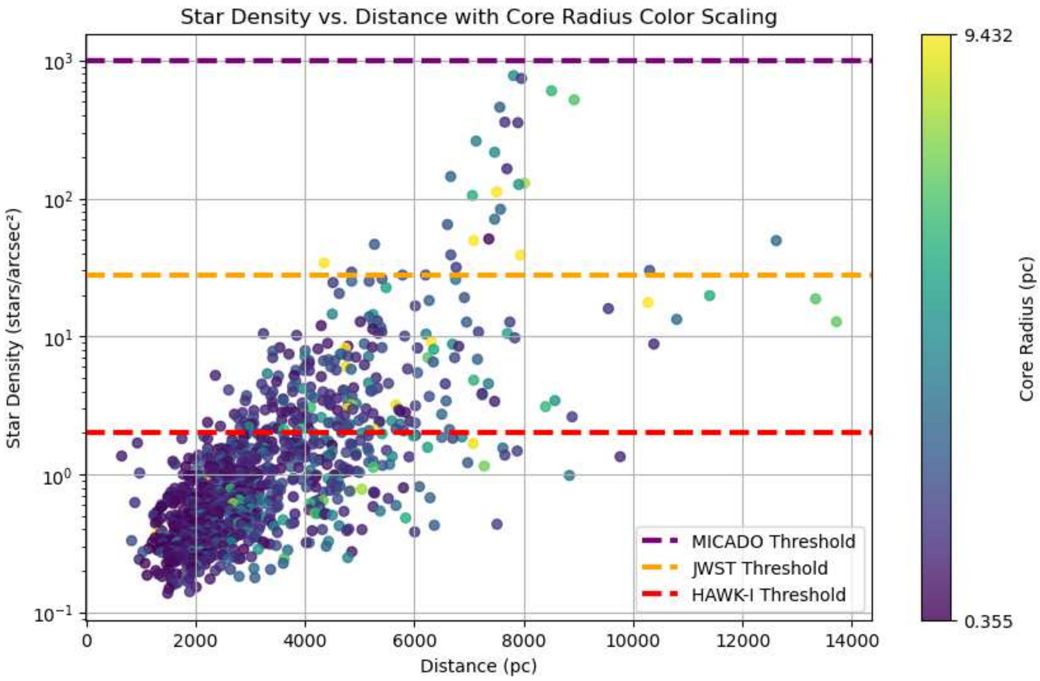

Figure 3.8.: Star density vs. distance for all clusters in the dataset with color scheme based on core radius size. Threshold lines for MICADO, JWST, and HAWK-I are shown as dashed lines, representing the maximum star density each instrument can effectively handle based on their crowding limits.

zone, which covers regions beyond HAWK-I's detection range for densities below 2 stars per arcsec^2; the blue MICADO zone, spanning densities between 28 and 1000 stars per arcsec^2; and the light blue MICADO Efficiency Zone. The MICADO Efficiency Zone highlights the range where JWST's resolution suffices, but MICADO offers significantly faster observations due to its larger mirror, making it ideal for intermediate-density clusters.

In the J-band, 546 clusters fall within HAWK-I's range, 293 within JWST's range, 185 in the MICADO Efficiency Zone, and 25 reach MICADO's density range. In the Ks-band, 394 clusters are in HAWK-I's range, 445 in JWST's range, 185 in the MICADO Efficiency Zone, and 25 in MICADO's range. These values demonstrate that HAWK-I is best suited for observing nearby, low-density clusters, while JWST is effective for more distant, less crowded regions. MICADO, however, excels in observing dense clusters, particularly in regions like the Galactic Center, and significantly reduces observation time compared to JWST for clusters in the MICADO Efficiency Zone.

These plots highlight the critical role of MICADO on the ELT for studying dense and distant star clusters. While HAWK-I and JWST provide valuable capabilities, MICADO's ability to observe high-density fields at greater distances is indispensable for IMF research in the Galactic Center and in general beyond the solar neighborhood.

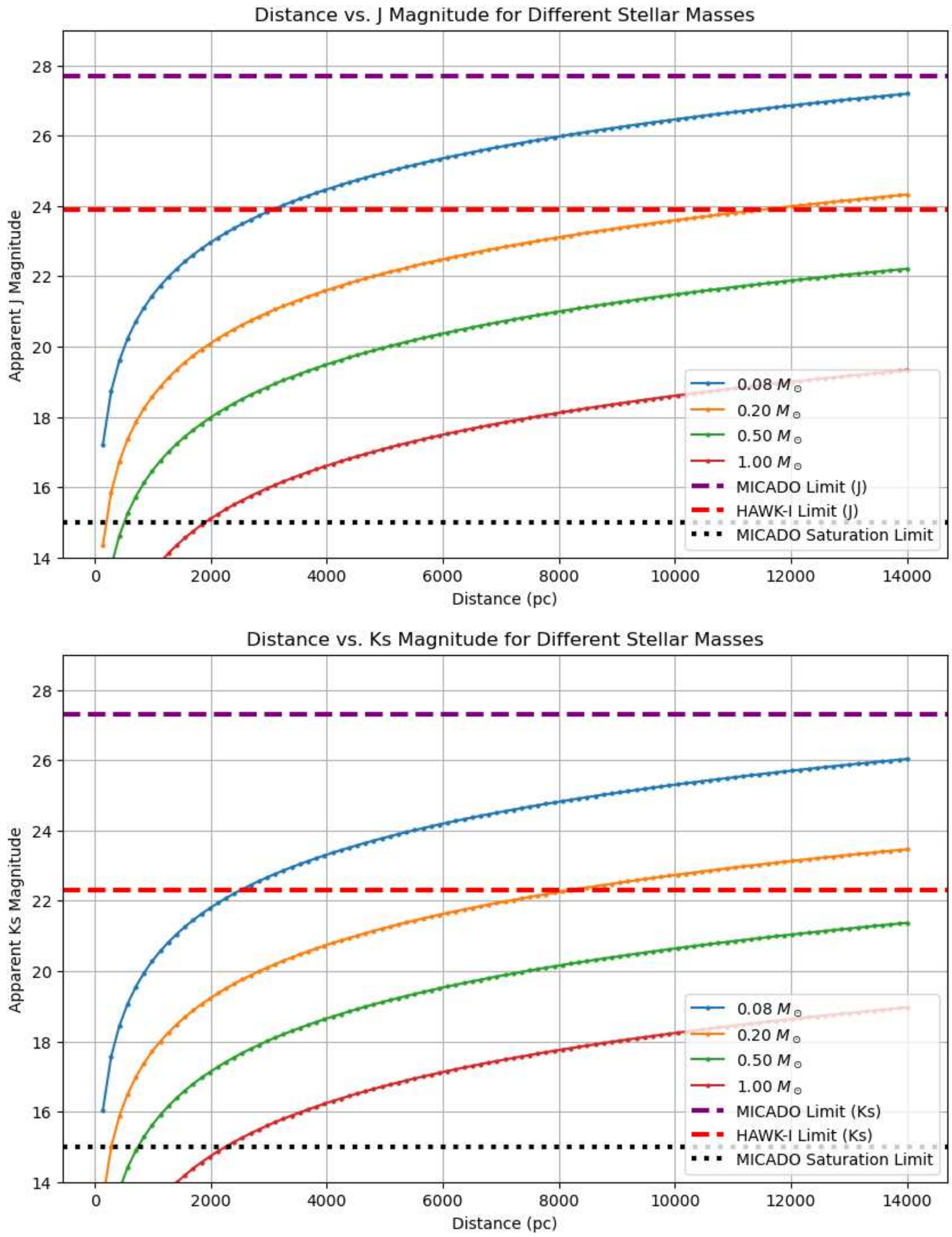

Figure 3.9.: Distance vs. Apparent Magnitude for Different Stellar Masses in the J and Ks bands. The plots illustrate how apparent magnitudes change with distance for stars of masses (0.08, 0.2, 0.5, and 1.0 $M_\odot$), along with the sensitivity thresholds for MICADO when using MCAO (27.7 mag in J and 27.3 mag in Ks, purple) and HAWK-I (23.9 mag in J and 22.3 mag in Ks, red), as well as the MICADO saturation limit (black dotted line at 15 mag for both bands). Stars brighter than the saturation limit cannot be measured by MICADO without saturating the detector and should instead be observed with HAWK-I. Conversely, MICADO is essential for observing faint stars in distant clusters due to its superior sensitivity.

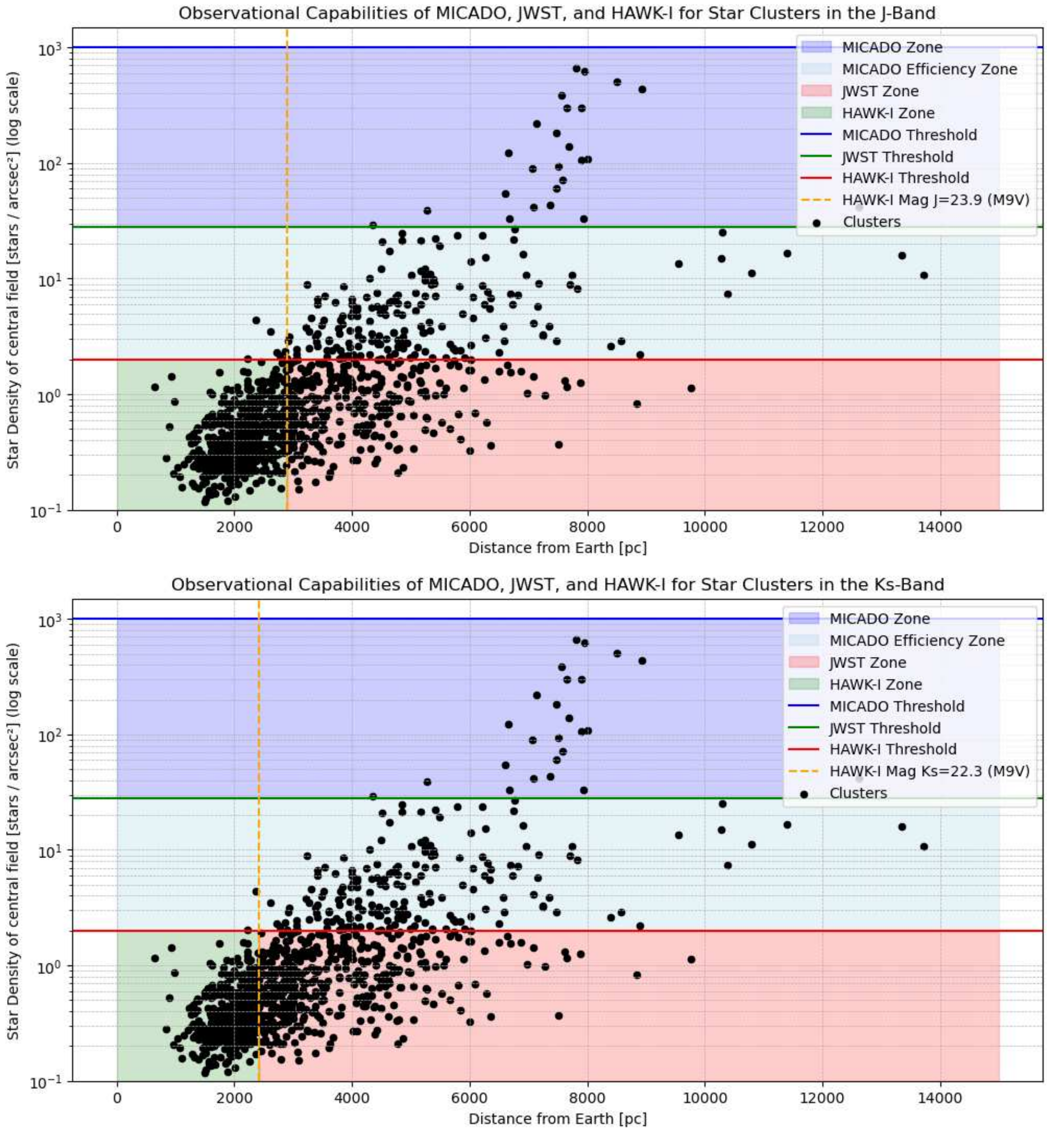

Figure 3.10.: Observational Capabilities of MICADO, JWST, and HAWK-I for Star Clusters in the J- and Ks-Bands. The plots show the relationship between star density in the central detector and distance for all clusters in the dataset. Threshold lines for MICADO (blue), JWST (red), and HAWK-I (green) denote the maximum star densities each instrument can effectively handle, while the orange dashed line represents HAWK-I's detection limit in distance (J Mag = 23.9 and Ks Mag = 22.3 for an M9V star). The blue, red and green shaded regions indicate crowding-limited zones where MICADO, JWST, and HAWK-I are the recommended instruments, respectively. The MICADO Efficiency Zone (light blue) is the area where observations require only the resolution of JWST but can be conducted significantly faster with MICADO due to its larger mirror. These plots demonstrate MICADO's ability to observe clusters with higher star densities and at greater distances, while HAWK-I and JWST complement this capability in their respective zones.

3.3. The IMF Handbook for ELT Observations

The **IMF Handbook for ELT Observations** is a comprehensive reference tool that guides the selection and analysis of open star clusters for Initial Mass Function (IMF) studies with the ELT. It is publicly available on GitHub at `https://github.com/MaxiKoe/IMF_MasterProject`. This handbook includes detailed pages for each of the 1047 open star clusters identified as observable with the ELT, particularly suited for high-resolution observations using MICADO.

Each page of the handbook follows a standardized layout, allowing for quick evaluation of each cluster's characteristics. Examples of three handbook pages are provided in Appendix A.2. The key components included are as follows:

- **Cluster Information**: The basic properties of each star cluster are summarized, including the cluster name, total mass, distance, number of stars, and estimated age. Essential parameters like core radius, tidal radius, galactic coordinates, and apparent magnitudes for reference stars (a G2 and an M9 star) in both J and Ks filters are also provided.

- **Suggested Instrument (Based on Crowding Distance)**: A recommended instrument is suggested for each cluster, depending on the crowding distance, which determines the spatial resolution required to resolve individual stars. There is a table with the crowding distances for MICADO (ELT), NIRCam (JWST) and HAWK-I (VLT). MICADO is recommended for clusters with the highest stellar density within its field of view, while HAWK-I should be sufficient for the observation of around 50% of the clusters in the handbook.

- **Simulated Images**: High-resolution simulated images in J and Ks bands give a visual preview of what the cluster would look like through MICADO on the ELT. It's important to say, that these images reflect only the central detector of MICADO, not the whole field of view. These images highlight the density and distribution of stars in the two different filters. It's a preview of the observations and should help to and understand potential observational challenges related to star crowding and magnitude limits. Also FITS files for all cluster simulations in both filters are provided on Github: `https://github.com/MaxiKoe/IMF_MasterProject`.

- **Position Plot**: This plot displays the Milky Way in galactic coordinates, with the cluster's position marked as a yellow dot. It provides an immediate spatial reference, allowing astronomers to understand the cluster's location relative to the Galactic plane.

- **Stellar Distribution Plot**: This plot illustrates the density distribution of stars within the cluster, marking the core and tidal radii and indicating MICADO's field of view (FoV) for spatial reference. It helps to visualize the spatial extent of the cluster and provides insight into how well the MICADO instrument can capture different regions, from the dense core to the outer tidal radius.

- **SNR Plot**: The Signal-to-Noise-Ratio (SNR) plot shows the average Signal-to-Noise Ratio (SNR) for different spectral types in both the J and Ks bands. The SNR is plotted on a logarithmic scale, with red dots representing the avarage SNR values for the J-Filter, and blue dots for the Ks filter. Green and red dashed lines indicate the SNR thresholds of 5 and 10, commonly used as benchmarks for reliable detection of the stars. The plot allows a direct assessment of detectability across various stellar types and highlights how observational feasibility decreases with fainter stars, particularly for later spectral types.

Each page is structured to provide astronomers with quick access to both quantitative and visual data about each cluster. The handbook should be a help to make decisions regarding observational planning and the choice of instrumentation for IMF based observations in the future.

For the thesis including descriptions of all 1047 clusters would be impossible of course. Therefore three clusters are described as representative examples to illustrate the variety in cluster characteristics and observational challenges: NGC 2447 (3.3.1) a nearby cluster, Kronberger 85 (3.3.2) a distant cluster, and vdBergh-Hagen 222 (3.3.3) a very dense cluster. These examples demonstrate the diversity within the Milky Way's clusters and highlight specific factors to consider in planning ELT observations.

3.3.1. Near Cluster Example: NGC 2447

NGC 2447, located at a distance of 1037 pc, has a total mass of 925 $M_\odot$. Its estimated number of stars is approximately 2100, calculated via the Kroupa IMF, and it has an age of 478 Myr. Figure 3.11 shows simulated images of NGC 2447 in the J and Ks bands, illustrating the spatial distribution and brightness of individual stars within MICADO's field of view. A relatively low number of stars (around 30) is visible, with large distances between them. The crowding distance for MICADO is 467 px, for JWST 61 px, and for HAWK-I 18 px, making HAWK-I the ideal instrument for observations of this cluster.

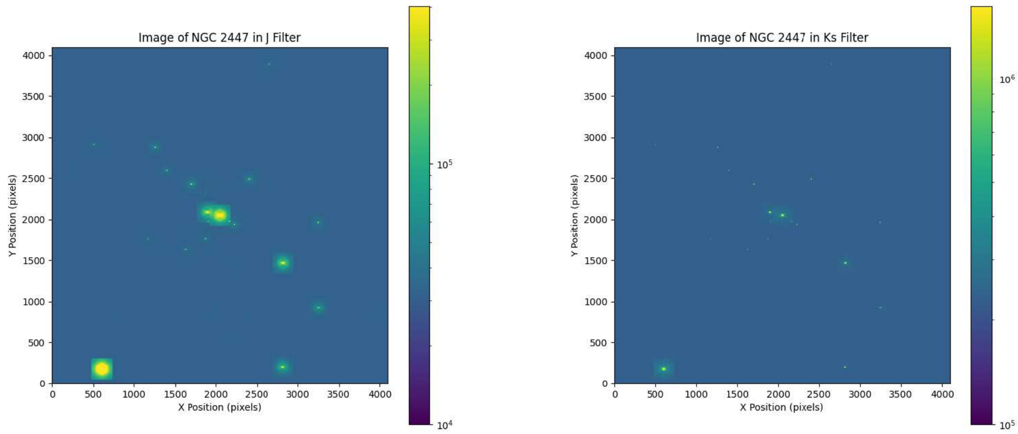

Figure 3.11.: Simulated J-band and Ks-band images of NGC 2447. A relatively low number of stars (around 30) is visible, with large distances between them. The cluster, with its low stellar density and close proximity to Earth, serves as an example where HAWK-I is sufficient for observation.

The stellar distribution plot (Left plot of Figure 3.12) displays the layout of stars in the cluster, marked with the core and tidal radii, and highlights the central area covered by MICADO's field of view. Although *NGC 2447* is not a massive cluster, it has a relatively large core radius of 2.73 pc and a tidal radius of 14.69 pc.

The SNR distribution plot (Right plot of Figure 3.12) indicates how signal-to-noise ratios vary across different magnitudes in the cluster for MICADO observations. High SNRs are achieved for brighter stars, while fainter stars exhibit lower SNRs. For this cluster, even the lowest-mass stars would achieve an SNR around 1000 using MICADO, with all stars bright enough to be observable with HAWK-I. An M9 star, for instance, has an apparent magnitude of 21.67 mag in the J band and 20.48 mag in the Ks band.

If we were to observe this nearby cluster with MICADO, it would require 103 MICADO fields to cover the core radius and 2900 fields to capture the entire tidal radius, equating to a total observation time of approximately 120 days of continuous observing (assuming 1 hour per field). Thus, *NGC 2447* is not an optimal target for IMF studies using the ELT. Instead, observations with HAWK-I at the VLT are recommended, as neither limiting magnitude nor crowding issues are expected for this nearby, relatively sparse cluster.

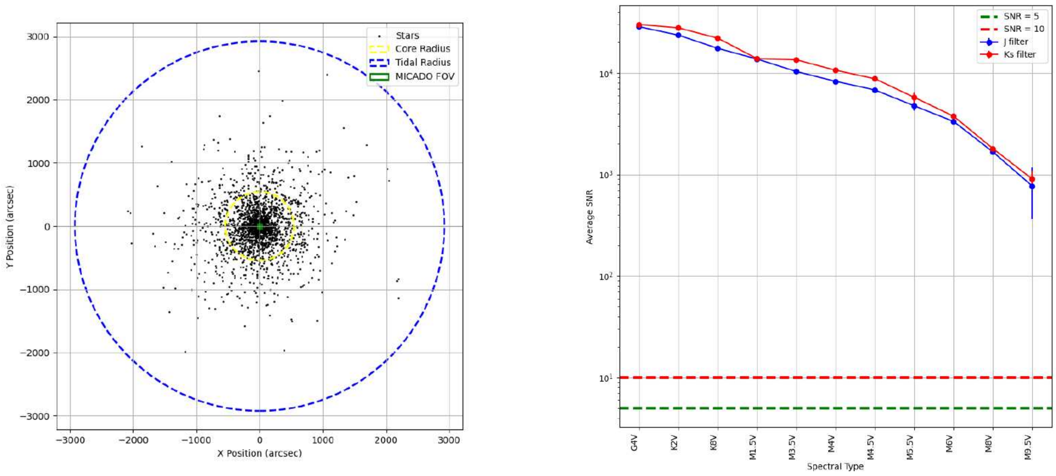

Figure 3.12.: On the left: Stellar distribution in NGC 2447, including the tidal radius, core radius, and MICADO FoV. Observing this nearby cluster with MICADO would require 103 fields to cover the core radius and 2900 fields for the entire tidal radius.
On the right: SNR distribution across magnitudes for NGC 2447. Even the lowest-mass stars achieve an SNR of approximately 1000 with MICADO, and all stars are bright enough to be observable with HAWK-I.

3.3.2. Far Cluster Example: Kronberger 85

Kronberger 85, located at a distance of approximately 10380 pc, has a total mass of around 2506 $M_\odot$. Because of its considerable distance, Kronberger 85 serves as an example of why a larger instrument like the ELT is advantageous for IMF studies, as its stars are observable with sufficient sensitivity using MICADO. This cluster showcases the potential of the ELT for observing faint stars in distant clusters that would otherwise be challenging to study in detail.

In Figure 3.13, simulated images in the J and Ks bands show that MICADO can effectively capture the cluster's members even at this distance. Although Kronberger 85's stars are generally fainter than those in closer clusters, MICADO's high sensitivity allows for the detection of both brighter and moderately faint stars, supporting detailed IMF analysis.

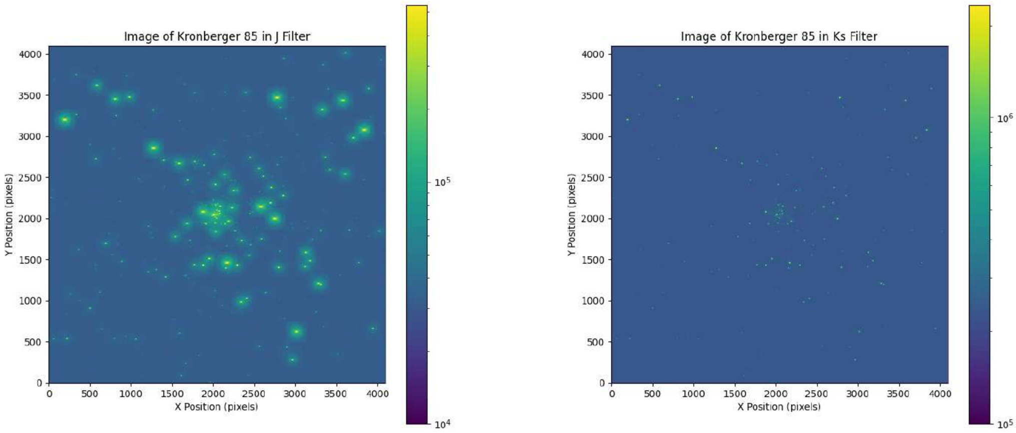

Figure 3.13.: Simulated J-band and Ks-band images of Kronberger 85. MICADO's high sensitivity allows for the detection of both brighter and moderately faint stars in this distant cluster.

The stellar distribution plot (Left plot of Figure 3.14) illustrates the spatial structure of Kronberger 85. The core radius of this cluster is relatively small at 1.46 pc, and MICADO's field of view, marked on the plot, covers a substantial portion of this region. A single MICADO pointing is sufficient to cover the core radius; however, for the much larger tidal radius (27 pc), more than 100 observations would be required.

The SNR distribution plot (Right plot of Figure 3.14) reveals that while MICADO generally provides sufficient signal-to-noise ratios across a range of stellar magnitudes, there is notable variability in the SNR for low-mass stars. The average SNR for these fainter stars remains above the minimum detection threshold of SNR $>$ 10, but the standard deviation is high, indicating a wide spread in SNR values for low-mass stars. This suggests that, although most low-mass stars are detectable, individual measurements may vary in quality. This variability is important for IMF studies, as inconsistent measurements of low-mass stars could introduce noise into the IMF analysis and impact the reliability of low-mass population data.

If we consider potential instruments for observing *Kronberger 85*, both crowding and sensitivity are key factors. At this distance, HAWK-I lacks the necessary sensitivity to detect faint stars in the cluster, making it unsuitable. The crowding distance for MICADO is 84 px, and for JWST, it is 10 px, which enables both instruments to handle the star density in the cluster's core. While MICADO's larger field of view covers the core radius in a single pointing, NIRCam on JWST may be better suited for observing the cluster's more extended tidal regions.

In summary, *Kronberger 85* demonstrates how MICADO on the ELT enables IMF studies of clusters many kiloparsecs away. Its distance and faint stellar population emphasize MICADO's high sensitivity, making it possible to observe distant clusters that would otherwise be inaccessible with smaller telescopes.

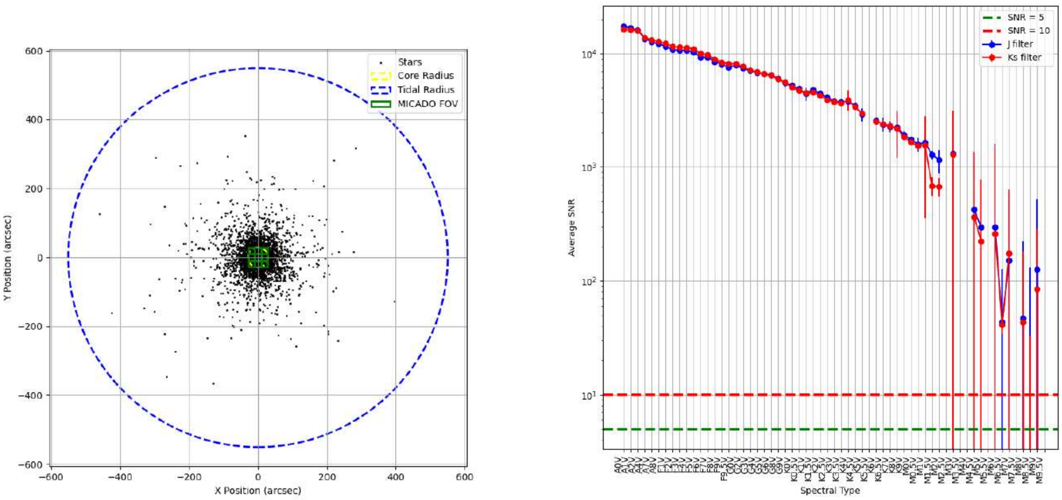

Figure 3.14.: On the left: Stellar distribution in Kronberger 85 with tidal radius, core radius, and MICADO FoV. A single MICADO pointing is sufficient to cover the core radius; however, for the much larger tidal radius (27 pc), more than 100 observations would be required.
On the right: SNR distribution across magnitudes for Kronberger 85. The plot highlights that, while MICADO provides sufficient SNR across most magnitudes, the variability in SNR for low-mass stars could affect the precision of IMF studies.

3.3.3. Dense Cluster Example: vdBergh-Hagen 222

vdBergh-Hagen 222, situated at a distance of 7813 pc, is a dense and massive open cluster with a total mass of approximately 717,794 $M_\odot$. With over 1.6 million stars, this cluster has an exceptionally high core density of 33.224 stars/arcsec^2, presenting a challenging test case for MICADO's resolving power in highly crowded environments. The core radius measures 4.77 pc (125.93 arcsec), while the tidal radius extends to 44.52 pc (1175.34 arcsec).

In the J- and Ks-band images (Figure 3.15), the central region reveals a densely packed stellar population, with stars frequently overlapping due to the extreme crowding. This dense environment highlights the necessity of high spatial resolution to separate individual stars and reduce photometric contamination, a task that only advanced instrumentation like MICADO can approach.

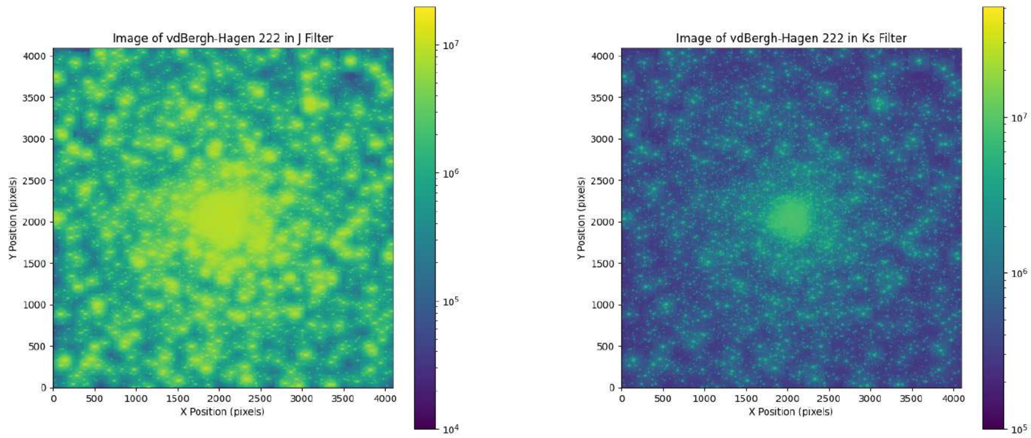

Figure 3.15.: Simulated J-band and Ks-band images of vdBergh-Hagen 222. The central region reveals a densely packed stellar population, with stars frequently overlapping due to the extreme crowding.

The stellar distribution plot (Left plot of Figure 3.16) illustrates the spatial structure of vdBergh-Hagen 222. The core is highly concentrated, but MICADO's field of view covers only a small fraction of it. Observing the entire cluster, particularly beyond the core, would require a significant number of fields (>450) due to its extensive tidal radius.

The SNR distribution plot (Right plot of Figure 3.16) demonstrates that while bright stars achieve high signal-to-noise ratios, the SNR for fainter, low-mass stars shows considerable variability and a high standard deviation. This variability is exacerbated by the crowding, especially near the cluster core, where blending effects hinder accurate photometry of individual stars. This high standard deviation in SNR for lower-mass stars poses a significant challenge, as it impacts the reliability of measurements needed for IMF studies.

In summary, *vdBergh-Hagen 222* represents an exceptionally dense and crowded cluster where the ELT's advanced capabilities are required just to distinguish individual stars.

Although MICADO's high spatial resolution allows for some level of separation, this cluster is not an ideal target for IMF studies due to extreme crowding, high SNR variability among low-mass stars, and the extensive number of fields required to cover its tidal radius. The crowding distance for MICADO is 9 px, only marginally above the operational limit of 8 px. Even with MICADO, detailed analysis of faint stars in such a densely populated environment would be extremely challenging. This cluster serves as an example of the limitations that even state-of-the-art instruments face in ultra-dense regions, underlining the need to carefully select clusters that balance scientific goals with observational feasibility.

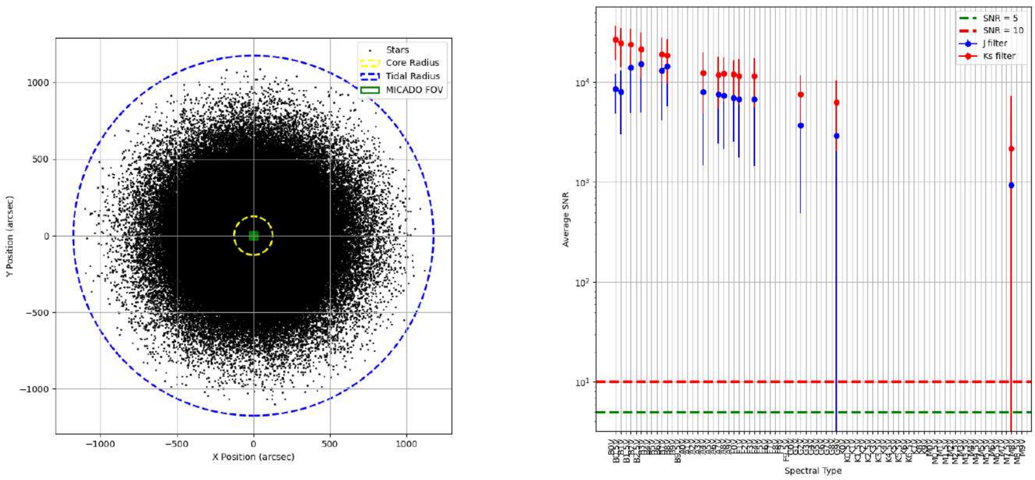

Figure 3.16.: On the left: Stellar distribution in vdBergh-Hagen 222 with tidal radius, core radius, and MICADO FoV. Observing the entire cluster, particularly beyond the core, would require a significant number of fields (>450) due to its extensive tidal radius.
On the right: SNR distribution across magnitudes for vdBergh-Hagen 222. Although MICADO's high spatial resolution allows for some level of separation, this cluster is not an ideal target for IMF studies due to extreme crowding, high SNR variability among low-mass stars, and the extensive number of fields required to cover its tidal radius.

4. Discussion

This chapter discusses the limitations and challenges encountered in photometric analysis of dense star clusters with the ELT, particularly focusing on MICADO observations. It also addresses the possibilities that high-resolution ELT observations open up for studying IMF variability in the Milky Way's core. The chapter concludes by identifying clusters that would benefit most from ELT observations and estimating the observational effort required for such studies.

4.1. Challenges for Future IMF Studies Using the ELT

The Extremely Large Telescope (ELT) brings unprecedented capabilities to the study of stellar populations and the Initial Mass Function (IMF) in dense star fields. However, the unique design and operation of the ELT also introduce new challenges, particularly related to its segmented mirror, crowding in dense fields, and field of view limitations. Addressing these challenges will be critical for optimizing the ELT's potential in IMF research.

4.1.1. Photometry with segmented mirrors

Segmented mirrors, like those used in advanced telescopes such as the ELT, bring the advantage of increased mirror size and improved resolution. However, this design also introduces complexities in photometry. One of the main challenges is the segmented mirror's complex Point Spread Function (PSF), which can lead to artifacts in the image. These artifacts often manifest as "false stars" or multiple detections around bright stars, making it difficult to accurately identify and measure them in dense clusters.

In Figure 4.1, we can see how these PSF artifacts impact automated star detection. The DAOStarFinder algorithm [Stetson, 1987], for instance, struggles to correctly interpret the PSF of very bright stars, often detecting multiple "false" stars around them. In contrast, faint stars tend to be less affected by this issue, as their lower brightness does not interact as significantly with the segmented PSF, allowing for more accurate detection.

This issue with bright stars complicates photometric measurements by introducing noise and potentially distorting the perceived distribution of stars in crowded fields. For this problem advanced algorithms are needed that can better distinguish between real stars and PSF artifacts, especially around bright stars.

Future developments in photometric software aim to address these challenges by refining detection algorithms to handle segmented PSFs, thus reducing the likelihood of false detections around bright stars and enhancing the quality of data in crowded star fields.

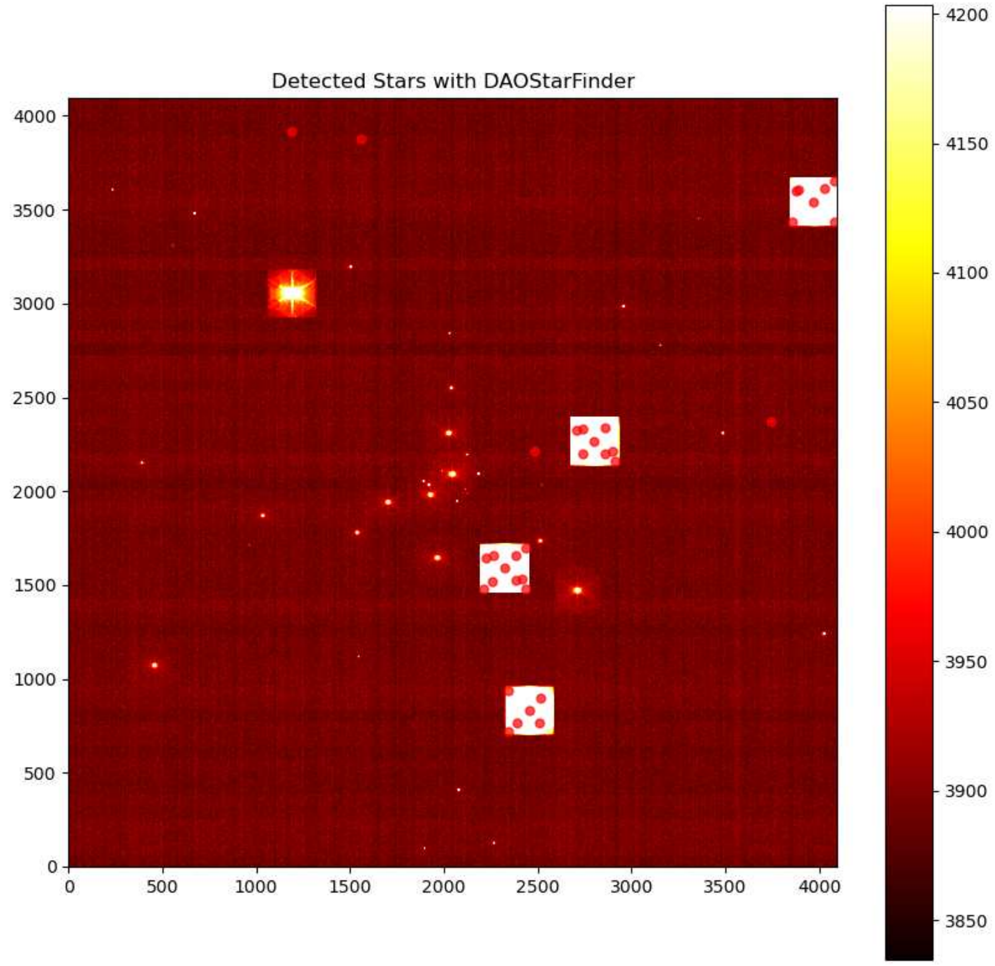

Figure 4.1.: Detected stars using DAOStarFinder, showing multiple false detections around bright stars due to the segmented mirror's PSF structure.

Advanced versions of PSF modeling, machine learning-driven detection, and improved de-blending algorithms are expected to be integrated into photometric tools. It is essential that such software be available by the time of the ELT's first light in 2028, as the lack of these capabilities would make accurate photometry extremely challenging. The success of IMF studies and other detailed stellar observations with the ELT will depend a lot on these advancements.

4.1.2. Crowding in Dense Stellar Fields

Crowding remains a significant challenge for photometry in dense stellar environments, such as the centers of star clusters or galactic cores. The ELT, with its high spatial resolution, improves upon the VLT's ability to resolve crowded regions, yet it still faces challenges in the densest fields. In crowded areas, stars appear close together or even overlap, making it difficult to isolate and accurately measure individual stars.

The dense arrangement of stars can lead to photometric blending, which in turn impacts the accuracy of measurements. While aperture photometry may struggle in such crowded regions, PSF subtraction photometry offers a potential solution. This method can help separate overlapping stars, but, as noted earlier, requires a precise PSF model—a challenging requirement for the ELT due to its segmented mirror design. Accurately modeling the PSF in crowded regions is thus essential for maximizing the ELT's capability to study the IMF in dense stellar fields.

4.1.3. Field of View Limitations

Although the ELT's resolving power allows for high-precision observations in crowded regions, its field of view (FoV) is relatively small compared to the size of many star clusters or extended galactic areas. For instance, MICADO, the ELT's first-light camera, has a FoV of 53x53 arcseconds. This means that capturing an entire star cluster often requires multiple pointings, which can add significant observation time.

This limitation affects the completeness of data for large clusters and adds challenges for observation time and planning. Multi-pointing and mosaicking techniques will be needed to fully cover large clusters, making some IMF studies more complex and time-consuming to plan. This added complexity will need to be carefully considered when planning large-scale projects with the ELT.

4.2. Opportunities for IMF Studies

The ELT opens new pathways for studying the Initial Mass Function (IMF) across different environments, especially in regions where traditional instruments face significant challenges.

One of the major opportunities lies in exploring the low-mass end of the IMF, capturing stars with a lower mass than 0.1 $M_\odot$ in the Milky Way aswell in nearby galaxies. MICADO's sensitivity extends to faint objects but does not reach the brown dwarf regime for extragalactic targets. This limiting magnitude means that the very low-mass stars, crucial for a complete picture of the IMF, remain observable only within the Milky Way [Leschinski and Alves, 2020].

In the Galactic center, MICADO can be used to study the IMF in an extreme environment with high stellar densities, tidal forces, and intense radiation fields. These conditions are thought to influence the formation and mass distribution of stars. By resolving individual stars in this crowded environment, the ELT can improve our understanding of how the IMF may vary due to environmental factors, contributing valuable data for star formation theories in such dense regions.

Beyond the Milky Way, the ELT enables IMF studies in nearby galaxies, such as the Magellanic Clouds. The lowest reliably observable mass in the Large Magellanic Cloud will be around 0.1 $M_\odot$ for clusters with densities below 10^3 stars arcsec^{-2}. Extending further, in regions up to approximately 2 Mpc, MICADO can resolve stars down to roughly 2 $M_\odot$ [Leschinski and Alves, 2020], allowing for detailed examination of the high-mass end of the IMF, though excluding the full low-mass spectrum. Studying IMF variability in external galaxies, particularly those with different metallicities and star formation conditions, will help test whether the IMF is universal or varies systematically across galactic environments.

4.3. Future Observations and Recommendations

With the capabilities of the ELT, it's essential to prioritize target clusters carefully to maximize scientific output and manage observation time effectively. This section recommends a list of clusters near the Galactic Center as optimal targets for IMF studies, while also acknowledging practical challenges and possible solutions for future observations.

Table 4.1 provides a list of 11 clusters in the Galactic Center region chosen for their moderate core and tidal radii and manageable core densities. Massive clusters, such as FSR 0033 with a mass of 132,000 $M_\odot$, are included alongside lower-mass clusters like BDSB 114. These clusters represent ideal candidates for IMF studies, as they allow ELT observations to explore the IMF in environments with high stellar density and unique conditions that could influence star formation.

The observation times listed are based on the assumption that one MICADO field of view requires approximately 1 hour of observing time. Thus, the total observation time is estimated from the number of MICADO pointings needed to cover both the core and the tidal radius of each cluster. The IMF handbook and accompanying table provide comprehensive data—mass, size, density, and observation time estimates—making it easier to select the best targets for future ELT studies.

Observing an entire cluster, including both core and tidal regions, with MICADO on the ELT presents challenges. MICADO's field of view (53 x 53 arcseconds) means multiple fields are needed to cover the large spatial extent of these clusters, resulting in extended observation times. For instance, some clusters in our list would require over 100 hours to cover the tidal radius, making full observation of each cluster's extent impractical.

To overcome the challenges of observing dense and distant star clusters, using multiple instruments could be beneficial. MICADO, with its high resolution, is ideal for studying the crowded cores of clusters, especially near the Galactic Center where stars are densely packed. HAWK-I, on the other hand, has a wider field of view, which makes it effective for observing the outer, less dense areas of clusters. However, HAWK-I lacks the sensitivity to detect low-mass stars and brown dwarfs at the distance of the Galactic Center, which limits its ability to fully study the IMF.

JWST's NIRCam could also play an important role in IMF studies. NIRCam has high sensitivity and at the same time a much larger field of view than MICADO, making it well-suited for detecting low-mass stars and brown dwarfs at larger distances. Its infrared capabilities allow it to observe through dust, which is useful for studying clusters in dusty regions like the Galactic Center. By combining data from MICADO, HAWK-I, and NIRCam, a more complete picture of the IMF could be achieved, especially for clusters where HAWK-I's sensitivity falls short.

In summary, MICADO on the ELT is essential for observing the dense cores of clusters in the Galactic Center. HAWK-I can cover the outer regions, but it is limited in detecting the faintest stars. JWST's NIRCam could complement these observations by helping detect low-mass stars and observing in dusty regions. The IMF handbook and table provide guidance to help choose the best instruments and strategies, ensuring that ELT's resources are used effectively for IMF studies.

Cluster	**Tidal Mass ($M_\odot$)**	**Obs. Time (Core)**	**Obs. Time (Tidal)**
FSR 0033	132,000	1h	136h
DBSB 176	57,000	1h	138h
Dutra-Bica 28	47,000	3h	39h
FSR 1763	52,000	4h	178h
DBSB 169	21,000	2h	144h
BDSB 166	18,500	5h	70h
DBSB 171	14,000	2h	107h
Ruprecht 133	10,400	7h	134h
FSR 0043	3,600	2h	180h
BDSB 165	674	2h	25h
BDSB 114	285	1h	29h

Table 4.1.: Recommended Galactic Center Clusters for ELT Observations, ordered by Tidal Mass.

5. Conclusion

The Initial Mass Function (IMF) is a key concept for understanding how stars form and how galaxies evolve. This thesis created a framework for studying the IMF by simulating observations of open star clusters with future instruments, particularly the Extremely Large Telescope (ELT) and its MICADO camera. As part of this project, an IMF handbook was developed to help guide the selection of clusters and observation strategies for high-resolution IMF studies. The ultimate goal is to gain better insights into the low-mass end of the IMF, which is still not well understood.

- **IMF Handbook and Thesis Outputs:** This work analyzed more than 1,000 open star clusters, focusing on their structure, distances, and star densities. The results are summarized in the *IMF Handbook for ELT Observations*, which provides recommendations for using the ELT. Additional resources, such as the cluster table and MICADO simulation files (J- and Ks-Band), were also created and are available on GitHub: `https://github.com/MaxiKoe/IMF_MasterProject`. These tools will help future researchers plan IMF observations more effectively.
- **MICADO's Role:** MICADO is essential for studying distant and crowded star clusters, such as those of the Galactic Center. Its high spatial resolution makes it possible to identify and measure individual stars, even in the dense cores of clusters. This ability is crucial for studying cluster structure and the IMF, especially in regions where other instruments struggle with crowding.
- **Synergies with Other Instruments:** MICADO works best when combined with other instruments like HAWK-I and JWST. MICADO excels in observing dense cluster cores, while HAWK-I is better for nearby, less crowded regions. JWST, with its larger field of view, is useful for studying more distant and diffuse clusters. Together, these instruments could provide a more complete picture of star clusters across different environments.
- **Remaining Challenges:** While MICADO is highly capable, challenges remain, particularly in ultra-dense clusters where crowding limits even its resolution. Additionally, MICADO's segmented mirror design can introduce complications for photometry. These issues highlight the need for careful planning and target selection to get the best results.

In summary, this thesis provides valuable tools and insights for IMF studies with the ELT. By combining MICADO's advanced capabilities with other instruments such as

HAWK-I and NIRCam, astronomers will be better equipped to explore the IMF across a variety of galactic environments. The outputs of this project, including the IMF Handbook, cluster data, and simulation files, will help address key questions about star formation and the less understood low-mass end of the IMF.

6. Acknowledgements

First and foremost, I would like to express my sincere gratitude to my supervisor, Dr. Kieran Leschinski, for proposing this fascinating research project. This thesis would not have been possible without his careful guidance and expertise. He was always available to offer his help whenever I had questions during my research.
I also wish to thank Dr. David Gruber and his team at Planetarium Südtirol for giving me the opportunity to gain practical experience in an astronomical environment during my studies.
Furthermore, I am grateful to everyone at the Institute of Astrophysics in Vienna, including professors and fellow students, who have supported me throughout these years.
I am deeply thankful to my parents, Klaus and Irene, for their unwavering moral and financial support during my studies. Thank you for giving me all the time I needed to complete this journey. Without you, this would never have been possible. Lastly, I want to thank my dear brother, Paul, for his help with some programming work.

Bibliography

[Astropy, 2013] Astropy (2013). Astropy: A community python package for astronomy. *Astronomy & Astrophysics*, 558:A33.

[Bastian et al., 2010] Bastian, N., Covey, K. R., and Meyer, M. R. (2010). A Universal Stellar Initial Mass Function? A Critical Look at Variations. , 48:339–389.

[Binney and Merrifield, 1998] Binney, J. and Merrifield, M. (1998). *Galactic Astronomy*.

[Bruzual and Charlot, 2003] Bruzual, G. and Charlot, S. (2003). Stellar population synthesis at the resolution of 2003. *Monthly Notices of the Royal Astronomical Society*, 344:1000–1028.

[Burrows et al., 2001] Burrows, A., Hubbard, W. B., Lunine, J. I., and Liebert, J. (2001). The theory of brown dwarfs and extrasolar giant planets. *Reviews of Modern Physics*, 73(3):719–765.

[CDS, 2023] CDS (2023). Global survey of star clusters in the milky way vii. tidal parameters and mass function. `https://cdsarc.cds.unistra.fr/viz-bin/cat/J/A+A/672/A187#/browse`. Accessed: 2024-10-17.

[Chabrier, 2003] Chabrier, G. (2003). Galactic Stellar and Substellar Initial Mass Function. , 115(809):763–795.

[Davies et al., 2010] Davies, R., Ageorges, N., Barl, L., Bedin, L. R., Bender, R., Bernardi, P., Chapron, F., Clenet, Y., Deep, A., Deul, E., Drost, M., Eisenhauer, F., Falomo, R., Fiorentino, G., Förster Schreiber, N. M., Gendron, E., Genzel, R., Gratadour, D., Greggio, L., Grupp, F., Held, E., Herbst, T., Hess, H. J., Hubert, Z., Jahnke, K., Kuijken, K., Lutz, D., Magrin, D., Muschielok, B., Navarro, R., Noyola, E., Paumard, T., Piotto, G., Ragazzoni, R., Renzini, A., Rousset, G., Rix, H. W., Saglia, R., Tacconi, L., Thiel, M., Tolstoy, E., Trippe, S., Tromp, N., Valentijn, E. A., Verdoes Kleijn, G., and Wegner, M. (2010). MICADO: the E-ELT adaptive optics imaging camera. In McLean, I. S., Ramsay, S. K., and Takami, H., editors, *Ground-based and Airborne Instrumentation for Astronomy III*, volume 7735 of *Society of Photo-Optical Instrumentation Engineers (SPIE) Conference Series*, page 77352A.

[Davies et al., 2021] Davies, R., Hörmann, V., Rabien, S., Sturm, E., Alves, J., Clénet, Y., Kotilainen, J., Lang-Bardl, F., Nicklas, H., Pott, J. U., Tolstoy, E., Vulcani, B., and MICADO Consortium (2021). MICADO: The Multi-Adaptive Optics Camera for Deep Observations. *The Messenger*, 182:17–21.

[ESO, 2021] ESO (2021). *HAWK-I User Manual*. VLT-MAN-ESO-14800-3486.

[European Southern Observatory (ESO), 2024] European Southern Observatory (ESO) (2024). ESO Extremely Large Telescope (ELT) Project Overview. `https://www.eso.org/public/teles-instr/elt/`. Available on the ESO website.

[Ginsburg, nd] Ginsburg, A. (n.d.). Imf python package. `https://github.com/keflavich/imf`.

[Hainaut, 2005] Hainaut, O. (2005). Signal-to-noise in ccd astronomy. European Southern Observatory (ESO).

[Just et al., 2023] Just, A., Piskunov, A. E., Klos, J. H., Kovaleva, D. A., and Polyachenko, E. V. (2023). Global survey of star clusters in the Milky Way. VII. Tidal parameters and mass function. , 672:A187.

[Kharchenko et al., 2013] Kharchenko, N. V., Piskunov, A. E., Schilbach, E., Röser, S., and Scholz, R.-D. (2013). Global survey of star clusters in the milky way. i. the pipeline and fundamental parameters in the second quadrant. *Astronomy Astrophysics*, 558:A53.

[King, 1962] King, I. R. (1962). The structure of star clusters. i. an empirical density law. *The Astronomical Journal*, 67:471.

[Kissler-Patig et al., 2008] Kissler-Patig, M., Pirard, J.-F., Casali, M., Moorwood, A., Ageorges, N., Alves de Oliveira, C., Baksai, P., Bedin, L., Bemmerer, D., Biereichel, P., Delabre, B., Dorn, R., Esteves, R., Finger, G., Gojak, D., Huster, G., Jung, Y., Koch, F., Lombini, M., Mehrgan, L., Meyer, M., Nicolini, G., Reyes, J., Siebenmorgen, R., Silber, A., Stegmeier, J., Vaytet, N., and Wegerer, E. (2008). Hawk-i: A new wide-field 1- to 2.5-m imager for the vlt. *Astronomy & Astrophysics*, 491:941–950.

[Kroupa, 2001] Kroupa, P. (2001). On the variation of the initial mass function. , 322(2):231–246.

[Leschinski and Alves, 2020] Leschinski, K. and Alves, J. (2020). The future of IMF studies with the ELT and MICADO. I. The local Universe as a resolved IMF laboratory. , 639:A120.

[Leschinski et al., 2020] Leschinski, K., Buddelmeijer, H., Czoske, O., Verdugo, M., Verdoes-Kleijn, G., and Zeilinger, W. (2020). ScopeSim: a flexible general purpose astronomical instrument data simulation framework in Python. In Guzman, J. C. and Ibsen, J., editors, *Software and Cyberinfrastructure for Astronomy VI*, volume 11452 of *Society of Photo-Optical Instrumentation Engineers (SPIE) Conference Series*, page 114521Z.

[Mamajek, 2013] Mamajek, E. E. (2013). A modern mean dwarf stellar color and effective temperature sequence. `https://www.pas.rochester.edu/~emamajek/EEM_dwarf_UBVIJHK_colors_Teff.txt`.

[Marks et al., 2012] Marks, M., Kroupa, P., Dabringhausen, J., and Pawlowski, M. S. (2012). Evidence for top-heavy stellar initial mass functions with increasing density and decreasing metallicity. , 422(3):2246–2254.

[MWSC, 2013] MWSC (2013). Milky way star cluster (mwsc) catalogue. `https://heasarc.gsfc.nasa.gov/w3browse/all/mwsc.html`. Accessed: 2024-10-17.

[Offner et al., 2014] Offner, S. S. R., Clark, P. C., Hennebelle, P., Bastian, N., Bate, M. R., Hopkins, P. F., Moraux, E., and Whitworth, A. P. (2014). The Origin and Universality of the Stellar Initial Mass Function. In Beuther, H., Klessen, R. S., Dullemond, C. P., and Henning, T., editors, *Protostars and Planets VI*, pages 53–75.

[Rieke et al., 2005] Rieke, M. J., Kelly, D. M., Horner, S. D., and et al. (2005). The near-infrared camera (nircam) for the james webb space telescope (jwst). In *Proceedings of SPIE*, volume 5904, page 1.

[Salpeter, 1955] Salpeter, E. E. (1955). The luminosity function and stellar evolution. *The Astrophysical Journal*, 121:161.

[Spiegel et al., 2011] Spiegel, D. S., Burrows, A., and Milsom, J. A. (2011). The Deuterium-burning Mass Limit for Brown Dwarfs and Giant Planets. , 727(1):57.

[Stetson, 1987] Stetson, P. B. (1987). DAOPHOT: A Computer Program for Crowded-Field Stellar Photometry. , 99:191.

[Vienna,] Vienna, A. Scopesim templates: Source templates for astronomical simulations. `https://github.com/AstarVienna/ScopeSim_Templates`.

A. Appendix

A.1. Code for Cluster Generation and Simulations

This appendix provides the Python code used to generate star clusters, simulate observations with the MICADO instrument, and perform photometry.

A.1.1. Cluster Generation

The following functions generate cluster properties, including masses (following the Kroupa IMF), positions (following the King profile), magnitudes, and spectral types of the member stars.

```
import numpy as np
from astropy.table import Table, join
from scipy.interpolate import interp1d
import imf
from scopesim_templates.stellar import cluster_utils as cu
from astropy.io import fits, ascii

def generate_cluster_masses(total_mass, imf_type):
    """Generate stellar masses for a cluster using a specified IMF
    (IMF package by keflavich: https://github.com/keflavich/imf)"""
    if imf_type.lower() == 'kroupa':
        return imf.make_cluster(total_mass)
    elif imf_type.lower() == 'salpeter':
        return imf.make_cluster(total_mass, massfunc='salpeter')
    elif imf_type.lower() == 'chabrier':
        return imf.make_cluster(total_mass, massfunc='chabrier')
    else:
        raise ValueError("IMF type must be 'kroupa', 'salpeter', or 'chabrier'.")

def interpolate_magnitudes(masses):
    """Interpolate J and Ks magnitudes based on stellar masses."""
    mass_data = np.array([20.2, 18.7, 17.7, 14.8, 11.8, 9.9, 7.3, 6.1, 5.4, 5.1,
                          4.7, 4.3, 3.92, 3.38, 2.75, 2.68, 2.18, 2.05, 1.98, 1.86,
                          1.93, 1.88, 1.83, 1.77, 1.81, 1.75, 1.61, 1.5, 1.46, 1.44,
                          1.38, 1.33, 1.25, 1.21, 1.18, 1.13, 1.08, 1.06, 1.03, 1.0,
                          0.99, 0.985, 0.98, 0.97, 0.95, 0.94, 0.9, 0.88, 0.86, 0.82,
```

```
                          0.78, 0.73, 0.7, 0.69, 0.64, 0.62, 0.59, 0.57, 0.54, 0.5,
                          0.47, 0.44, 0.4, 0.37, 0.27, 0.23, 0.184, 0.162, 0.123,
                          0.102, 0.093, 0.09, 0.088, 0.085, 0.08, 0.079, 0.078, 0.077,
                          0.076, 0.075])

    mj_data = np.array([-3.44, -3.3, -3.17, -2.8, -2.33, -2.03, -1.34, -1.09, -0.83,
                        -0.66, -0.54, -0.28, -0.16, 0.19, 0.59, 0.63, 0.95, 1.08,
                        1.19, 1.49, 1.65, 1.68, 1.74, 1.8, 1.81, 1.89, 1.98, 2.11,
                        2.24, 2.32, 2.4, 2.52, 2.76, 2.85, 3.05, 3.21, 3.26, 3.37,
                        3.47, 3.6, 3.66, 3.7, 3.73, 3.81, 3.9, 3.96, 4.14, 4.31,
                        4.39, 4.46, 4.7, 4.91, 5.1, 5.31, 5.59, 5.75, 5.82, 5.97,
                        6.19, 6.48, 6.59, 6.81, 7.01, 7.38, 7.93, 8.2, 8.8, 9.09,
                        9.72, 10.18, 10.47, 10.7, 10.88, 11.05, 11.46, 11.59,
                        11.75, 11.76, 12.12, 12.47])

    mks_data = np.array([-3.20, -3.073, -2.942, -2.587, -2.126, -1.848, -1.198,
                        -0.956, -0.708, -0.553, -0.376 -0.192, -0.075, 0.254,
                        0.621, 0.648, 0.949, 1.07, 1.07, 1.172,  1.447, 1.587,
                        1.607, 1.655, 1.702, 1.694, 1.756, 1.836, 1.941, 2.045,
                        2.116, 2.188, 2.291, 2.5, 2.579, 2.76, 2.915, 2.947, 3.043,
                        3.12, 3.236, 3.282, 3.319, 3.345, 3.41, 3.49, 3.53, 3.69,
                        3.82, 3.89, 3.93, 4.1, 4.25, 4.4, 4.56, 4.81, 4.95, 5.01,
                        5.15, 5.36, 5.64, 6.75, 5.98, 6.18, 6.55, 7.10, 7.36, 7.93,
                        8.2, 8.8,  9.22, 9.5, 9.7, 9.81, 9.92, 10.3, 10.4, 10.5,
                        10.55, 10.77,11])

    interp_func_j = interp1d(mass_data, mj_data, kind='linear',
    fill_value=(mj_data[-1], mj_data[0]), bounds_error=False)
    interp_func_ks = interp1d(mass_data, mks_data, kind='linear',
    fill_value=(mks_data[-1], mks_data[0]), bounds_error=False)

    mj_magnitudes = interp_func_j(masses)
    mks_magnitudes = interp_func_ks(masses)

    return mj_magnitudes, mks_magnitudes

def king_density(r, r_c, r_t, sigma_0):
    """Calculate the King density profile for a given radius."""
    term1 = (1 + (r / r_c)**2)**-0.5
    term2 = (1 + (r_t / r_c)**2)**-0.5
    return sigma_0 * (term1 - term2)**2

def compute_king_cdf(r_c, r_t, sigma_0, steps=1000):
```

```
    """Compute the cumulative distribution function (CDF) for the King profile."""
    r = np.linspace(0, r_t, steps)
    densities = king_density(r, r_c, r_t, sigma_0)
    cdf = np.cumsum(densities) * np.diff(r, prepend=0)
    cdf /= cdf[-1]
    return interp1d(cdf, r, bounds_error=False, fill_value=(r[0], r[-1]))

def sample_king_profile(r_c, r_t, sigma_0, n_stars):
    """Sample positions for stars based on the King profile."""
    cdf_func = compute_king_cdf(r_c, r_t, sigma_0)
    random_values = np.random.rand(n_stars)
    radii = cdf_func(random_values)
    angles = np.random.uniform(0, 2 * np.pi, n_stars)
    x = radii * np.cos(angles)
    y = radii * np.sin(angles)
    return x, y

def filter_stars_by_age(cluster_table, log_age):
    """Filter stars in the cluster based on the age and spectral type."""
    if log_age >= 9.0:
        spectral_types_to_keep = ['F', 'G', 'K', 'M']
    elif log_age >= 8.0:
        spectral_types_to_keep = ['A', 'F', 'G', 'K', 'M']
    elif log_age >= 7.0:
        spectral_types_to_keep = ['B', 'A', 'F', 'G', 'K', 'M']
    else:
        spectral_types_to_keep = ['O', 'B', 'A', 'F', 'G', 'K', 'M']

    filtered_table = cluster_table[np.isin([s[0] for s in cluster_table['Spectral Type']],
    spectral_types_to_keep)]
    return filtered_table

def create_cluster_table(total_mass, distance, imf_type, core_radius, tidal_radius,
norm_factor, log_age):
    # Generate cluster masses based on the IMF type
    cluster_masses = generate_cluster_masses(total_mass, imf_type)

    # Interpolate magnitudes for J and Ks bands
    j_magnitudes_absolute, ks_magnitudes_absolute = interpolate_magnitudes(cluster_masses)

    # Calculate apparent magnitudes for J and Ks bands
    j_magnitudes_apparent = j_magnitudes_absolute + 5 * np.log10(distance / 10)
    ks_magnitudes_apparent = ks_magnitudes_absolute + 5 * np.log10(distance / 10)
```

```
    # Generate star positions using the King profile
    x_positions, y_positions = sample_king_profile(core_radius, tidal_radius,
    norm_factor, len(cluster_masses))

    # Convert positions from parsecs to arcseconds
    x_positions_arcsec = x_positions / distance * 206265
    y_positions_arcsec = y_positions / distance * 206265

    # Assign spectral types based on cluster masses
    spectral_types = cu.mass2spt(cluster_masses)

    # Create an Astropy Table with all the calculated data
    cluster_table = Table([cluster_masses,
    j_magnitudes_absolute, j_magnitudes_apparent,
    ks_magnitudes_absolute, ks_magnitudes_apparent,
    x_positions, y_positions, x_positions_arcsec,
    y_positions_arcsec, spectral_types],
    names=['Mass', 'J Mag(abs)', 'J Mag(app)',
    'Ks Mag(abs)', 'Ks Mag(app)', 'X Position (pc)',
    'Y Position (pc)', 'X Position (arcsec)',
    'Y Position (arcsec)', 'Spectral Type'])

    # Filter stars based on the age of the cluster
    filtered_table = filter_stars_by_age(cluster_table, log_age)

    return filtered_table

def get_cluster_params(cluster_name, table):
    cluster_row = table[table['NAME'] == cluster_name]
    if len(cluster_row) == 0:
        raise ValueError(f"Cluster with name {cluster_name} not found.")

    params = {
        'total_cluster_mass': cluster_row['TIDAL_MASS'][0],
        'r_c': cluster_row['KING_CORE_RADIUS'][0],
        'r_t': cluster_row['KING_TIDAL_RADIUS'][0],
        'sigma_0': cluster_row['KING_NORM_FACTOR'][0],
        'cluster_distance': cluster_row['DISTANCE'][0],
        'log_age': cluster_row['LOG_AGE'][0],
        'gal_lon': cluster_row['GAL_LON'][0],
        'gal_lat': cluster_row['GAL_LAT'][0],
        'ra': cluster_row['RA'][0],
```

```
        'dec': cluster_row['DEC'][0],
        'num_stars_core': cluster_row['NUM_STARS_CORE'][0],
        'num_stars_micado': cluster_row['NUM_STARS_MICADO'][0],
        'num_stars_tidal': cluster_row['NUM_STARS_TIDAL'][0],
        'num_stars_centraldetector': cluster_row['NUM_STARS_CENTRALDETECTOR'][0],
        'star_density_tidal': cluster_row['STAR_DENSITY_TIDAL'][0],
        'star_density_core': cluster_row['STAR_DENSITY_CORE'][0],
        'star_density_centraldetector': cluster_row['STAR_DENSITY_CENTRALDETECTOR'][0],
        'pixels_per_star_micado': cluster_row['PIXELS_PER_STAR_MICADO'][0],
        'pixels_per_star_jwst': cluster_row['PIXELS_PER_STAR_JWST'][0],
        'pixels_per_star_hawki': cluster_row['PIXELS_PER_STAR_HAWKI'][0],
    }
    return params
```

A.1.2. MICADO Simulations

The code below demonstrates how to simulate cluster observations with the MICADO instrument using the ScopeSim package.

```
import scopesim as sim
from scopesim.source import source_templates as sim_tp

def simulate_micado(cluster_table, filter_name='J'):
    """Simulate an observation with the MICADO instrument."""
    micado = sim.OpticalTrain("MICADO")
    src = stars(filter_name,
                cluster_table[f'{filter_name} Mag(app)'],
                cluster_table['Spectral Type'],
                cluster_table['X Position (arcsec)'],
                cluster_table['Y Position (arcsec)'])

    micado.cmds['!DET.width'] = 4096
    micado.cmds['!DET.height'] = 4096
    micado.cmds['!OBS.dit'] = 60
    micado.cmds['!OBS.ndit'] = 60

    if filter_name == 'J':
        micado.cmds['!OBS.filter_name_fw1'] = "J"
        micado.cmds['!OBS.filter_name_fw2'] = "open"
    elif filter_name == 'Ks':
        micado.cmds['!OBS.filter_name_fw1'] = "open"
        micado.cmds['!OBS.filter_name_fw2'] = "Ks"
    else:
        raise ValueError("Invalid filter name. Choose 'J' or 'Ks'.")
```

```
    micado.observe(src)
    hdus = micado.readout()[0]
    return hdus, micado
```

A.1.3. Photometry and Analysis

The following code performs rectangular aperture photometry on simulated MICADO images, extracting flux and signal-to-noise ratios for stars.

```
import numpy as np

def perform_photometry(hdus, micado):
    """Perform aperture photometry on the simulated data."""
    data = hdus[1].data
    star_positions = Table({
        'x': micado._last_fovs[0].fields[0]['x'] * 250 + 2048,
        'y': micado._last_fovs[0].fields[0]['y'] * 250 + 2048,
        'spectral_type': micado._last_fovs[0].fields[0]['spec_types']
    })
    results = []
    ap0, ap1, ap2 = 7, 20, 30
    ndit = 25
    for row in star_positions:
        x, y, spt = int(row['x']), int(row['y']), row['spectral_type']
        im_cutout = data[y-ap2:y+ap2, x-ap2:x+ap2]
        sig, snr = aperture_photometry(im_cutout, ap0, ap1, ap2, ndit=ndit)
        results.append((x, y, spt, sig, snr))

    dtype = [('x', int), ('y', int), ('spectral_type', 'U10'), ('flux', float),
    ('snr', float)]
    results_array = np.array(results, dtype=dtype)
    results_table = Table(results_array)
    return results_table


def aperture_photometry(im, ap0=10, ap1=20, ap2=30, ndit=60, ron=10):
    """Perform aperture photometry on a given image cutout."""
    x0, y0 = im.shape[0] // 2, im.shape[1] // 2
    bg = np.copy(im)
    bg[y0-ap1:y0+ap1, x0-ap1:x0+ap1] = 0
    bg_median = np.median(bg[bg!=0])
    n_pix = (2 * ap0) ** 2
```

```
sig = np.sum(im[y0-ap0:y0+ap0, x0-ap0:x0+ap0] - bg_median)
noise_sig = sig
noise_sky = bg_median * n_pix
noise_ron = ron**2 * ndit * n_pix
noise = np.sqrt(noise_sig + noise_sky + noise_ron)
snr = sig / noise
return sig, snr
```

A.2. Cluster Example Pages from IMF Handbook

On the following three pages, the example cluster pages from the **IMF Handbook for ELT Observations** are included. A detailed description of the images can be found in the Results section of the thesis 3.3.

Cluster: NGC 2447

- **Total Mass:** 924.7 $M_\odot$
- **Number of Stars:** 2102
- **Distance:** 1037.0 pc
- **Core Radius:** 2.73 pc / 543.01 arcsec
- **Tidal Radius:** 14.69 pc / 2921.92 arcsec
- **Age:** 478.63 Myr
- **Galactic Longitude:** 240.051°
- **Galactic Latitude:** 0.149°
- **Core Density:** 0.002 stars/arcsec^2
- **App. Mag G2 & M9 (J):** 13.68 & 21.67
- **App. Mag G2 & M9 (Ks):** 13.31 & 20.48
- **Suggested Instrument:** HAWK-I

Instrument	Crowding Distance (px)
MICADO	476.2
JWST	61.4
HAWKI	18.0

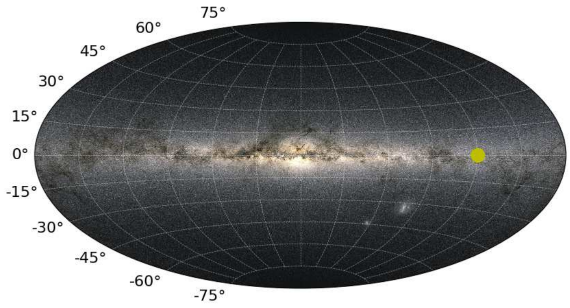

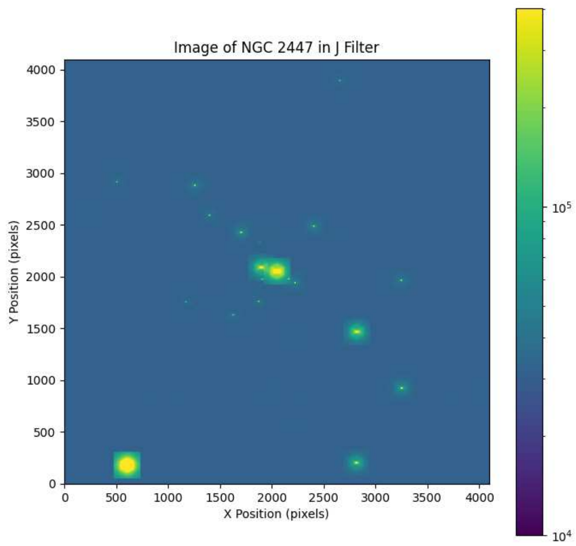

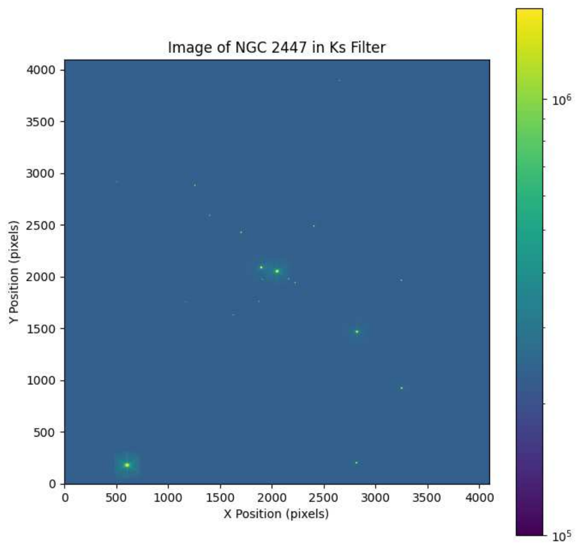

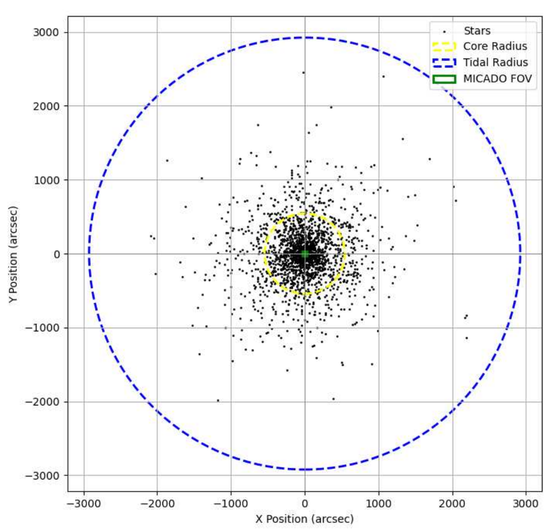

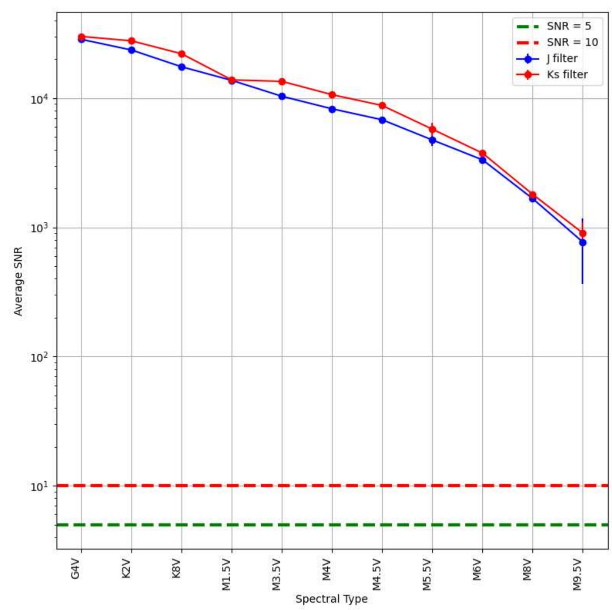

Cluster: Kronberger 85

- **Total Mass:** 2506.1 $M_\odot$
- **Number of Stars:** 5604
- **Distance:** 10380.0 pc
- **Core Radius:** 1.46 pc / 29.01 arcsec
- **Tidal Radius:** 27.71 pc / 550.64 arcsec
- **Age:** 316.23 Myr
- **Galactic Longitude:** 250.966°
- **Galactic Latitude:** -2.846°
- **Core Density:** 2.119 stars/arcsec^2
- **App. Mag G2 & M9 (J):** 18.68 & 26.67
- **App. Mag G2 & M9 (Ks):** 18.32 & 25.48
- **Suggested Instrument:** JWST or MICADO

Instrument	Crowding Distance (px)
MICADO	84.2
JWST	10.9
HAWKI	3.2

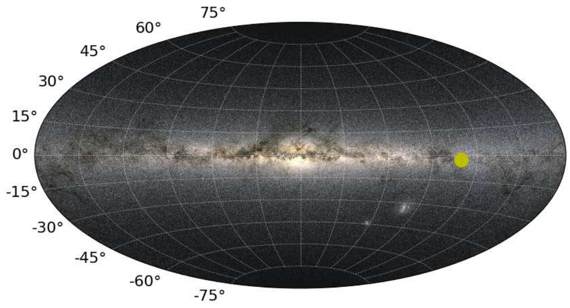

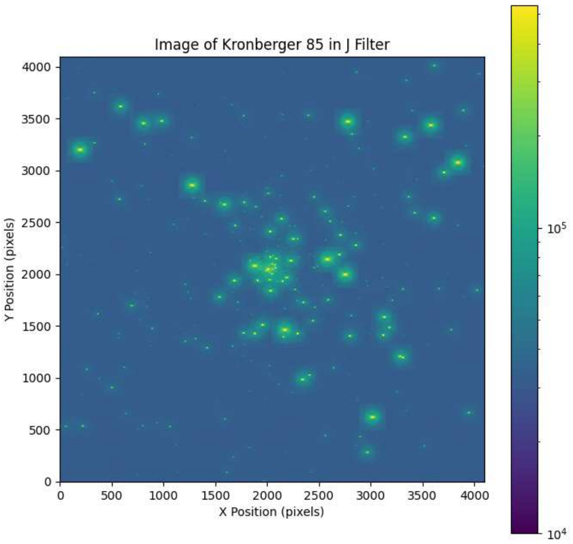

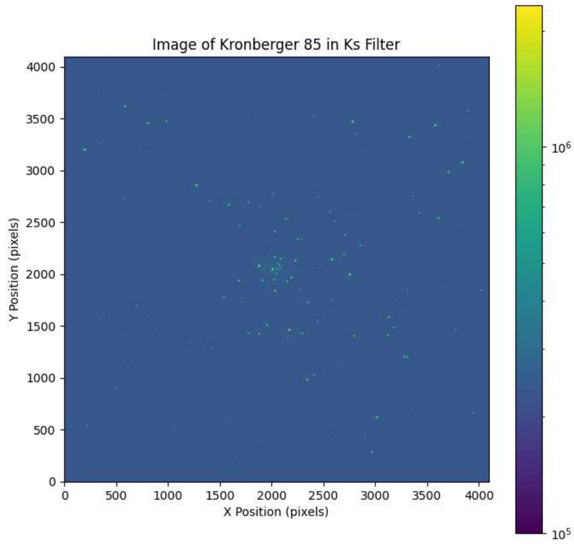

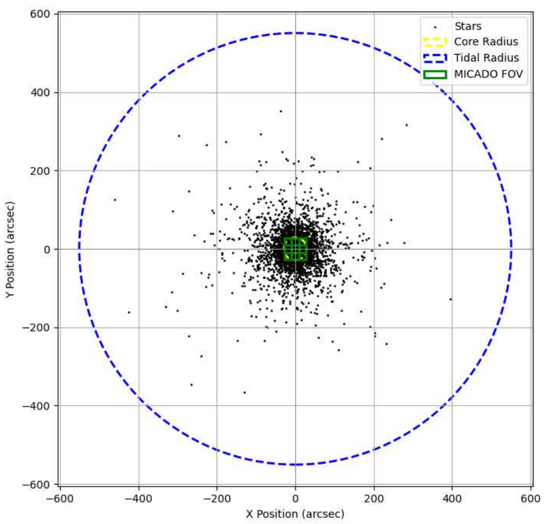

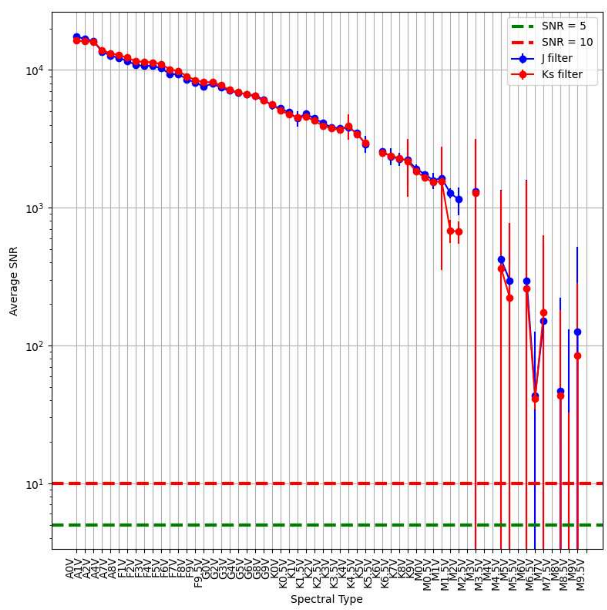

Cluster: vdBergh-Hagen 222

- **Total Mass:** 717794.3 $M_{\odot}$
- **Number of Stars:** 1655197
- **Distance:** 7813.0 pc
- **Core Radius:** 4.77 pc / 125.93 arcsec
- **Tidal Radius:** 44.52 pc / 1175.34 arcsec
- **Age:** 79.43 Myr
- **Galactic Longitude:** 349.114°
- **Galactic Latitude:** -0.443°
- **Core Density:** 33.224 stars/arcsec^2
- **App. Mag G2 & M9 (J):** 18.06 & 26.05
- **App. Mag G2 & M9 (Ks):** 17.70 & 24.86
- **Suggested Instrument:** MICADO

Instrument	Crowding Distance (px)
MICADO	9.0
JWST	1.2
HAWKI	0.3